

AD-A063 260

RAYTHEON CO BEDFORD MASS MISSILE SYSTEMS DIV
DIELECTRIC SPATIAL FILTER EXPERIMENTAL STUDY.(U)

NOV 78 J H POZGAY

UNCLASSIFIED

BR-10509

F/G 9/5

F19628-77-C-0111

NL

RADC-TR-78-248

| OF |
AD
A063 260



END
DATE
FILED
3--79
DDC

ADA 063260

(18) (19)
RADC TR-78-248
Final Technical Report
November 1978

LEVEL

12⁰⁵

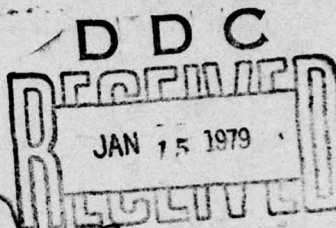


(6) DIELECTRIC SPATIAL FILTER EXPERIMENTAL STUDY.

Raytheon Company

(10) Jerome H. Pozgay

(12) 63p.



DDC FILE COPY

(9) Final technical
rept. Jan 77 - Jan 78

(15) FL9628-77-C-0111

Approved for public release; distribution unlimited.

(14) BR-10509

(16) 4600

(17) 14

ROME AIR DEVELOPMENT CENTER
Air Force Systems Command
Griffiss Air Force Base, New York 13441

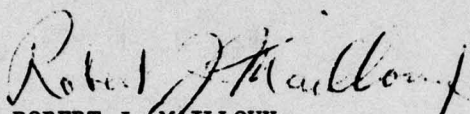
297 620 01 12 016

50B

This report has been reviewed by the RADC Information Office (OI) and is releasable to the National Technical Information Service (NTIS). At NTIS it will be releasable to the general public, including foreign nations.

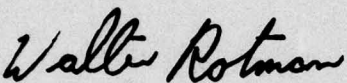
RADC-TR-78-248 has been reviewed and is approved for publication.

APPROVED:



ROBERT J. MAILLOUX
Alternate Contract Monitor
Electromagnetic Sciences Division

APPROVED:



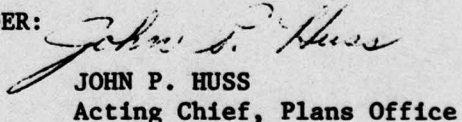
WALTER ROTMAN, Chief
Antennas & RF Components Branch
Electromagnetic Sciences Division

APPROVED:



WILLIAM R. BASCHNAGEL, Major, USAF
Assistant Chief
Electromagnetic Sciences Division

FOR THE COMMANDER:


JOHN P. HUSS
Acting Chief, Plans Office

If your address has changed or if you wish to be removed from the RADC mailing list, or if the addressee is no longer employed by your organization, please notify RADC (EEA) Hanscom AFB MA 01731. This will assist us in maintaining a current mailing list.

Do not return this copy. Retain or destroy.

UNCLASSIFIED

SECURITY CLASSIFICATION OF THIS PAGE (When Data Entered)

REPORT DOCUMENTATION PAGE		READ INSTRUCTIONS BEFORE COMPLETING FORM
1. REPORT NUMBER RADC-TR-78-248	2. GOVT ACCESSION NO.	3. RECIPIENT'S CATALOG NUMBER
4. TITLE (and Subtitle) DIELECTRIC SPATIAL FILTER EXPERIMENTAL STUDY		5. TYPE OF REPORT & PERIOD COVERED Final Technical Report Jan 77 - Jan 78
7. AUTHOR(s) Jerome H. Pozgay		6. PERFORMING ORG. REPORT NUMBER BR-10509 8. CONTRACT OR GRANT NUMBER(s) F19628-77-C-0111
9. PERFORMING ORGANIZATION NAME AND ADDRESS Raytheon Company Missile Systems Division Bedford MA 01730		10. PROGRAM ELEMENT, PROJECT, TASK AREA & WORK UNIT NUMBERS 62702F 46001429
11. CONTROLLING OFFICE NAME AND ADDRESS Deputy for Electronic Technology (RADC/EEA) Hanscom AFB MA 01731		12. REPORT DATE November 1978
14. MONITORING AGENCY NAME & ADDRESS(if different from Controlling Office) Same		13. NUMBER OF PAGES 62 15. SECURITY CLASS. (of this report) UNCLASSIFIED
		15a. DECLASSIFICATION/DOWNGRADING SCHEDULE N/A
16. DISTRIBUTION STATEMENT (of this Report) Approved for public release; distribution unlimited.		
17. DISTRIBUTION STATEMENT (of the abstract entered in Block 20, if different from Report) Same		
18. SUPPLEMENTARY NOTES RADC Project Engineer: Dr. Peter R. Franchi (EEA)		
19. KEY WORDS (Continue on reverse side if necessary and identify by block number) Angular Filters Sidelobe Suppression Low Sidelobe Antenna		
20. ABSTRACT (Continue on reverse side if necessary and identify by block number) This report summarizes the experimental investigation of a dielectric spatial filter. The spatial filter was designed under a previous effort. Specifically, the objectives were: To fabricate the spatial filter design under Contract F19628-76-C-0189; to test the completed filter with a linear array of polarization diverse circular elements. With respect to the test program the goal was to provide experimental confirmation of the filter concept and to investigate the array/filter interaction.		

(Cont'd)

The results of this study establish the effectiveness of such filters for reduction of sidelobes beyond 10° from broadside.

(b6)

UNCLASSIFIED

REF ID: A77-776-248
10-30-68

F19628-77-C-0111

EVALUATION

This report describes an experimental evaluation of dielectric slab angular filters. The synthesis techniques for deriving the filter parameters was done in an earlier work (RADC-TR-76-408). In this report the effectiveness of dielect slabs, used as an angular filter to reduce all sidelobes beyond ten to fifteen degrees from broadside, is clearly established. For example, a pair of grating lobes at 36° from broadside, that were originally just 6 dB below the mainbeam peak, are reduced to below 38 dB in the H plane and 28 dB in the E plane. The limitations on this type of filter, particularly those imposed by tolerances in the dielectric fabrication are well discussed. Some interesting effects of very close antenna-filter interaction are also examined.

Peter R Franchi

PETER R. FRANCHI
Antennas & RF Components Branch
Electromagnetic Sciences Division

ACCESS FOR	
NTIS	White Section <input checked="" type="checkbox"/>
DDC	Buff Section <input type="checkbox"/>
MANUFACTURED	
SPECIFICATION	
BY	
DISTRIBUTION/AVAILABILITY CODES	
Dist.	Spec. and/or Special
A	

UNCLASSIFIED

TABLE OF CONTENTS

	<u>Page</u>
I. INTRODUCTION AND SUMMARY	1
1.1 Filter Design Procedure	2
1.2 Multicomponent Microwave Dielectric Nonuniformities and Their Effect on Filter Performance and Testing	4
1.3 Filter Testing	5
II. EXPERIMENTAL INVESTIGATION OF PLANE WAVE SPATIAL FILTER USING SMALL RECTANGULAR PROBES	7
2.1 Filter Configuration and Test Facilities	7
2.2 Analysis of Filter Configuration	12
2.3 Measured Filter Response to TE and TM Plane Waves	19
2.3.1 Measured Filter Transmission Loss	19
2.3.2 Measured Relative Response	22
III. EXPERIMENTAL INVESTIGATION OF LINEAR ARRAY COUPLING TO DIELECTRIC SLAB SPATIAL FILTERS	28
3.1 Multipolarization Linear Array and Experimental Setup	28
3.2 Pattern Measurement Program	30
IV. CONCLUSIONS	44
APPENDIX A EMERSON & CUMING, INC. TEST REPORT	45
APPENDIX B DIELECTRIC SPATIAL FILTER COUPLING TO PLANAR ARRAYS OF CIRCULAR ELEMENTS	49
REFERENCES	54

v
UNCLASSIFIED

UNCLASSIFIED

LIST OF ILLUSTRATIONS

<u>Figure</u>		<u>Page</u>
1	Preliminary Eleven-Layer Filter Design	2
2	Transmission of Fields Generated by X-Directed Magnetic Current - Preliminary Filter Electrical Design	3
3	Experimental Filter Configuration	8
4	Filter Retainer	9
5	Raytheon Compact Range Facility	10
6	Final Design Configuration	12
7	TE Power Transmission Coefficient - Final	13
8	TM Power Transmission Coefficient - Final	13
9	TE Power Transmission Coefficient - Filter 1 ($f_o = 9.5 \text{ GHz}$)	15
10	TE Power Transmission Coefficient - Filter 2 ($f_o = 9.5 \text{ GHz}$)	16
11	TM Power Transmission Coefficient - Filter 1 ($f_o = 9.5 \text{ GHz}$)	17
12	TM Power Transmission Coefficient - Filter 2 ($f_o = 9.5 \text{ GHz}$)	18
13	Spatial Pulse Function Generator	20
14	$F(x', u_o, 0)$ versus $2x'/\lambda$ for 10° Passband	21
15	Filter 1 TE Response - 9.41 GHz	23
16	Typical Sidelobe Structure for Filter Truncated at $\pm 10\lambda$	24
17	Filter 1 TM Response - 9.41 GHz	25
18	Filter 1 TE Response - Parameter Frequency	26
19	Filter 1 TM Response - Parameter Frequency	27
20	128 Element Multiple Polarization Linear Array	29
21	Array/Filter Mount	31
22	Effect of Independent Phase and Amplitude Error Buildup - Full Filter - Full Array - 9.5 GHz	31
23	Effects of Independent Phase Error - Line Source Model	32
24	Pattern Properties of 20λ Spatial Pulse Generator with Assumed Phase Error	34
25	H-Plane Modified Linear Array Pattern with and Without Filter 1, 9.5 GHz	35
26	H-Plane Modified Linear Array Pattern with Filter 1, 9.33 GHz	37

UNCLASSIFIED

LIST OF ILLUSTRATIONS (Cont.)

<u>Figure</u>		<u>Page</u>
27	H-Plane Modified Linear Array Pattern with Filter 1, 9.5 GHz	38
28	H-Plane Modified Linear Array Pattern with Filter 1, 9.69 GHz	39
29	H-Plane Modified Linear Array Pattern with Filter 2, 9.33 GHz	40
30	H-Plane Modified Linear Array Pattern with Filter 2, 9.5 GHz	41
31	H-Plane Modified Linear Array Pattern with Filter 2, 9.69 GHz	42
32	E-Plane Modified Linear Array Pattern with Filter 1, 9.5 GHz	43
B-1	Equivalent Transmission Line Network for Spectral Orders of Unit Cell Waveguide	50
B-2	H-Plane Realized Gain Pattern with and Without Preliminary Design Eleven-Layer Filter - 9.5 GHz - Array Matched to Free Space	50
B-3	H-Plane Realized Gain Pattern with Preliminary Design Eleven-Layer Filter - 9.5 GHz - Array Matched to Filter . . .	51
B-4	$1 - \Gamma ^2$ versus Array/Filter Separation for an Array Supporting Grating Lobe - Preliminary Design Eleven-Layer Filter - 9.5 GHz	52

viii
UNCLASSIFIED

UNCLASSIFIED

I. INTRODUCTION AND SUMMARY

This report summarizes the experimental investigation of a dielectric slab spatial filter. The spatial filter was designed under a previous effort (Reference 1). Specifically, the objectives were:

- To fabricate the spatial filter designed under Contract F19628-76-C-0189.
- To test the completed filter with a linear array of polarization diverse circular elements

With respect to the test program, the goal was to provide experimental confirmation of the filter concept and to investigate the array/filter interaction.

The dielectric spatial filter is an 11-layer sandwich composed of ECCO-FOAM PS, STYCAST HiK and STYCAST HiHiK. The design values of relative dielectric constant were 1.02, 5, 9.5, and 23. All materials were synthesized by Emerson & Cuming, Inc. who also performed the filter fabrication task. The actual dielectric constant values synthesized were in variance with the design values and required redesign of the filter using the numerical optimization procedure (Reference 1) during the materials synthesis process. A redesign sequence was anticipated and an optimized filter design configuration was obtained. However, variation in material properties within a single sheet of the target $\epsilon_r = 23$ dielectric resulted in a limitation of the experimental scope. This aspect of the program will be discussed in detail below.

Principally, the experimental program consisted of the measurement of array and single element patterns with and without the filter in place. The array used for this purpose was a polarization diverse linear row of circular radiators. The ability to electronically switch polarization provided both E and H plane data on filter coupling to planar arrays. The most significant result obtained from the filter/array measurements is that the filter may be positioned with respect to an array supporting grating lobes such that the reactive termination of the spurious beams increases the main beam gain. This will be treated fully below. A theoretical discussion of planar array coupling to dielectric slab spatial filters is given in Appendix B.

UNCLASSIFIED

UNCLASSIFIED

1.1 Filter Design Procedures

A general computer optimization procedure for dielectric slab spatial filters was developed under Contract F19628-76-C-0189 (Reference 1). A particular result of this effort was an electrical design for an 11-layer filter consisting of $\epsilon_r = 1.02, 5, 9.5$, and 23 dielectrics. This filter configuration is shown in Figure 1. The layer thicknesses are given with respect to free-space wavelength at center frequency (9.5 GHz). Over the 4 percent design

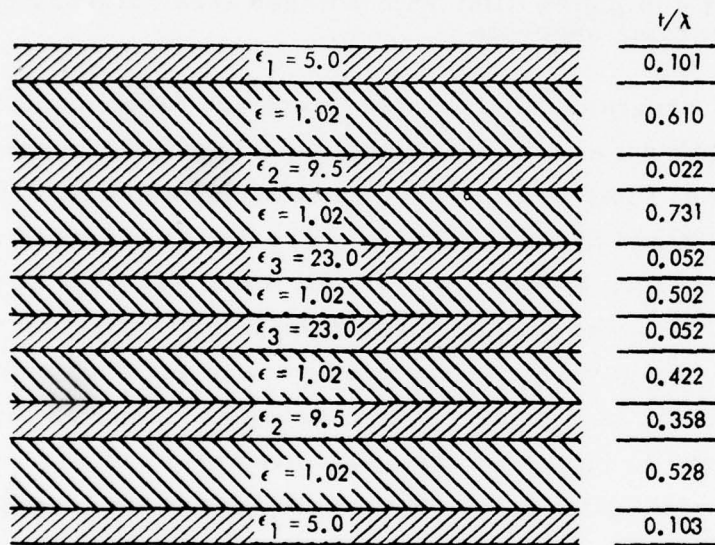


Figure 1 - Preliminary 11-Layer Filter Design

frequency band the filter has less than 0.15 dB insertion loss in the 10° spatial passband; and greater than 10 dB rejection beyond 24° from broadside for TE incidence (H-plane incidence with respect to an array). For TM incidence (E-plane), the stopband has greater than 10 dB rejection from 26° to 62° (the onset of the Brewster angle passband (Reference 1)). A contour plot of filter performance at center frequency is shown in Figure 2.

UNCLASSIFIED

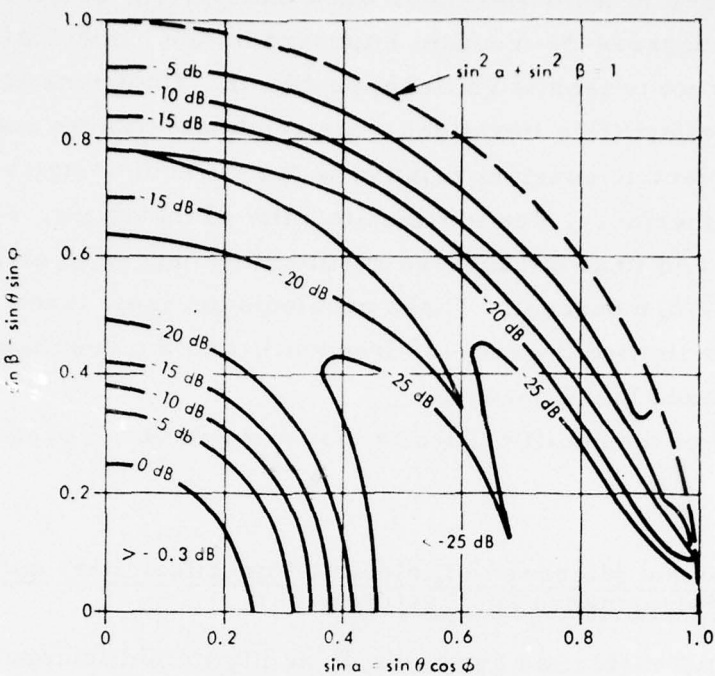


Figure 2 - Transmission of Fields Generated by X-Directed Magnetic Current-Preliminary Filter Electrical Design

It was initially proposed that the filter be comprised of synthesized multi-component dielectrics ($\epsilon_r = 5$ and 23), Alumina ($\epsilon_r = 9.5$) and low density foam. The multicomponent dielectrics are wide range materials which were selected by the optimizer due to the lack of either natural or ceramic materials with or in the range of these constants. The Alumina was selected by the optimizer due to its stable electrical properties. However, it was deemed to be more expedient and cost effective to obtain all materials from a single vendor - hence a wide range multicomponent dielectric was also selected for the 9.5 layer. Emerson & Cuming, Inc. was selected as the vendor for all dielectric materials and for the fabrication effort.

In anticipation of errors in the materials synthesis process (assumed to be of the order of ± 3 percent in ϵ_r for the high dielectric constant layers), a filter redesign procedure was developed. Briefly, the procedure required that the optimizer be exercised following materials synthesis and dielectric constant measurement at the design center frequency to obtain a new set of layer thicknesses which would result in filter performance roughly equal to that originally specified. Provided the errors were in the ± 3 percent range,

UNCLASSIFIED

only small changes in layer thickness were anticipated, and it was assumed that the limited degrees-of-freedom imposed on the numerical filter synthesis technique would not present significant problems. Unfortunately, at no point in the redesign effort (five iterations were required) was the maximum error in measured dielectric constant relative to the current design value less than 7 percent. Furthermore, due to nonuniformity of materials, surface grinding to intermediate and final thicknesses resulted in changes in dielectric constant as great as 6.6 percent. These problems severely taxed the optimizer (operating under limited degrees-of-freedom), and the resultant total filter thickness increased by 78 percent.

The impact of these difficulties is discussed in detail below and in Section 3.

1.2 Multicomponent Microwave Dielectric Nonuniformities and Their Effect on Filter Performance and Testing

The principal materials synthesis difficulty in multicomponent microwave dielectrics is evidently stratification of the particulate loading during pouring or injection processes (Reference 2). Consequently, within a single molded piece, dielectric constant may vary widely, depending on the manufacturer's techniques. Furthermore, depending on the pouring or injection procedure, flow streams may be nonlinear resulting in local, anisotropy, or change in dielectric constant with polarization. Clearly, such nonuniformities will depend strongly on the viscosity of the solution prior to curing, and, hence, degree of particulate loading.

In the instance that a single sheet of multicomponent dielectric forms an entire layer of a spatial filter, the principal area of concern is the average anisotropy of the slab. This, of course, applies primarily to filters for systems requiring multipolarization and/or wide angle filtering in all cut planes. However, for use with a large planar array or reflector systems, each layer of the filter must be comprised of several sheets. It is in this area that the greatest difficulty arises - small uniform or tapered phase errors over a significant percentage (but not all) of an antenna aperture will produce large errors in sidelobe levels within the spatial passband, and may occur without significantly altering main beam shape or pointing direction. Consequently, the principal advantage of molded dielectric sheets (which is that they are

UNCLASSIFIED

UNCLASSIFIED

available in very large dimensions relative to a wavelength at X-band) is lost. In order to minimize the effect of materials nonuniformities, the errors must be randomized by reducing the sheets to small tiles, thereby dramatically increasing the fabrication cost of the filter.

Each high dielectric constant layer of the filter consists of two sheets which are 23.19 in. x 5.65 in., giving an overall filter length of 46.38 in. This lengthwise splitting of the filter resulted in an insertion phase error of approximately 20° across the filter midplane due to the independent buildup of dielectric constant errors in each filter half. Consequently, array pattern measurements with the entire filter showed extreme sidelobe distortion in the spatial passband. It was, therefore, necessary to perform filter measurements on each filter half independently, which, due to the design of the test fixtures resulted in a limitation of the filter test program. Specifically, it was necessary to translate the array phase center to coincide with the lengthwise geometrical center of the filter half, leaving insufficient room in the fixture to allow filter tilt with respect to the array, or to allow an investigation of the effects of filter-to-array spacing. To compensate for the lack of experimental results for the filter-to-array spacing study, analytical results are presented in Section 3 and in Appendix B.

1.3 Filter Testing

Filter testing was performed at the Raytheon Compact Range Facility in Lowell, Massachusetts. The facility is a far field anechoic chamber with less than 0.3 dB amplitude taper and 2° phase distortion over a 4-ft³ quiet zone at 10 GHz. Typically, stray radiation is down 40 dB.

Filter testing was conducted with both a small rectangular waveguide probe and a linear polarization diverse phased array of loaded circular apertures. The small probe measurements (Section 2) provided a direct measurement of filter transmission coefficient for TM (E-plane) incidence, and a direct measurement of filter passband and skirt properties for TE incidence. The array measurements (Section 3) provided insight and quantitative data on array-to-filter coupling and demonstrated that for an array supporting grating lobes in the stopband of a spatial filter, a filter-to-array spacing can be determined which will result in an increase in main beam gain. Furthermore, it is demonstrated in Section 3 and Appendix B that a dielectric spatial filter

UNCLASSIFIED

UNCLASSIFIED

may be designed to match an existing array to free space, or, conversely, for a given spatial filter and array face geometry, an element matching structure can be determined which will maintain array gain in the presence of the filter. These results are an important extension of the conclusions given by Fante (Reference 3), and will therefore be discussed extensively in the sections mentioned above.

For theoretical discussions, the assumed time dependence is $e^{j\omega t}$.

UNCLASSIFIED

UNCLASSIFIED

II. EXPERIMENTAL INVESTIGATION OF PLANE WAVE SPATIAL FILTER USING SMALL RECTANGULAR PROBES

To determine the properties of the experimental filter, a thorough investigation of plane wave filtering was conducted using a 0.400 in. \times 0.900 in. open-ended rectangular waveguide probe with a 0.500 in. \times 1.000 in. flange. These investigations considered only relative pattern shape since the details of the filter mismatch at the probe could not be accounted by simple analytical arguments. For these measurements, the probe flange is butted directly against the filter back face.

2.1 Filter Configuration and Test Facilities

Figure 3 shows the configuration of the experimental filter. The filter is composed of 11 layers of low loss ($\tan \delta < 0.001$) dielectric. Six of the layers are wide range multicomponent materials, specifically Stycast HiK ($\epsilon_r \cong 5.0$), and Stycast HiHik ($\epsilon_r \cong 9.7$ and 23). The remaining slabs are EccoFoam PS ($\epsilon_r = 1.02+$). Layer thicknesses are given in inches, and the total thickness is 7.68 in. Cross-sectional dimensions are 46.38 in. \times 5.65 in. Total thickness deviation along the full length is less than 0.030 in. or 9° in air at 9.5 GHz. The thickness tolerance could be reduced significantly by replacing the foam layers with higher density foam (Emerson & Cuming, Incorporated recommends $\epsilon_r = 1.06$ for improved structural performance) or low loss honeycomb, such as HEXCEL HRH-10. The latter is recommended due to lower dielectric constant.

Each high dielectric constant layer is comprised of two sheets with the seam at the center. The foam layers have seams at locations other than the center. Appendix A gives the electrical properties of each sheet as measured by Emerson & Cumings Incorporated using a 45° interferometer. Data is taken with the polarization along the length of the sheet (0°) and perpendicular to the length of the sheet (90°).

UNCLASSIFIED

UNCLASSIFIED

CENTER SEAM OF Hi - ϵ LAYERS				
FILTER - 1		FILTER - 2		THICKNESS (in)
ϵ (TE)	ϵ (TM)	ϵ (TE)	ϵ (TM)	
5.03	4.85	4.93	4.82	0.466
1.02	1.02	1.02	1.02	2.438
9.72	9.63	9.63	9.72	0.268
1.02	1.02	1.02	1.02	1.874
*				
22.39	23.27	22.12	24.30	0.154
1.02	1.02	1.02	1.02	0.612 7.68 in
24.34	23.70	22.40	24.28	0.200
1.02	1.02	1.02	1.02	0.5
9.56	9.56	9.41	9.87	0.247
1.02	1.02	1.02	1.02	0.630
5.13	4.83	4.95	5.10	0.088
				46.38 in

Figure 3 - Experimental Filter Configuration

The filter retainer is shown in Figure 4. It consists of two sheets of 0.750 in. thick plywood and supporting members. The sheets form frames, with the filter inset 0.375 in. at its periphery. The frame overlap onto the filter face is 0.250 in. reducing the unobstructed filter cross-section to 45.88 in. x 5.15 in. A supporting member is located below the midseam to minimize stresses. The other support members provide structural integrity while allowing access to the filter edges.

The measurement program was conducted at the Raytheon Compact Range Facility. A sketch (side view) of the facility is shown in Figure 5. All measurements were taken with the filter in a horizontal position. The physical and performance, parameters for the facility are summarized in Table 1.

For the probe measurements, the entire backplane of the filter was covered with free space absorber to minimize scattering from the array support into the probe.

UNCLASSIFIED

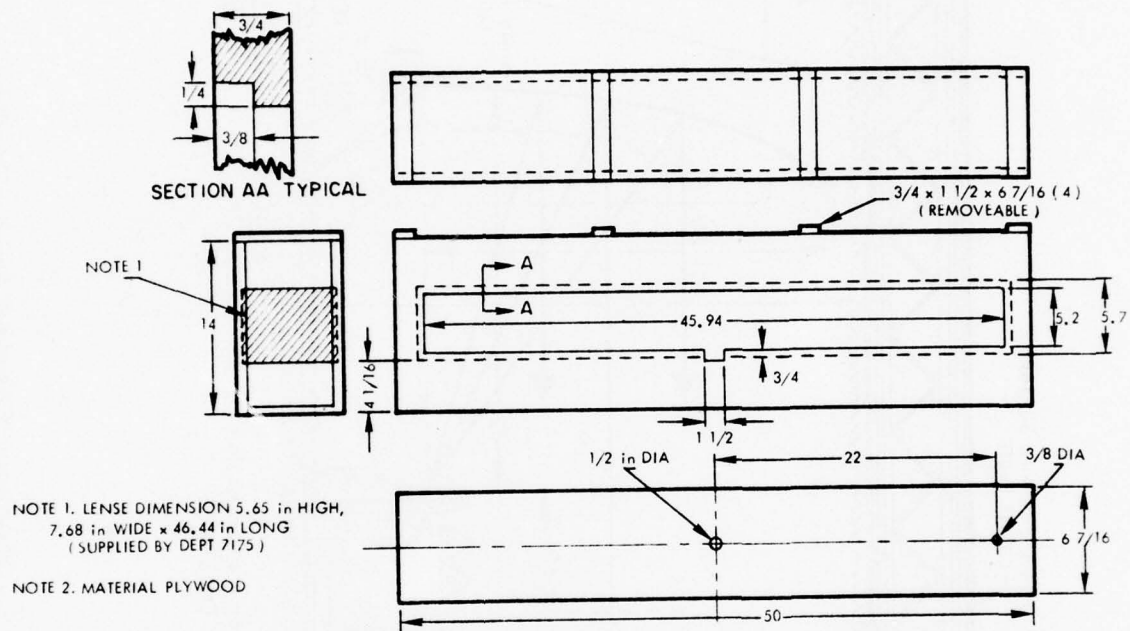
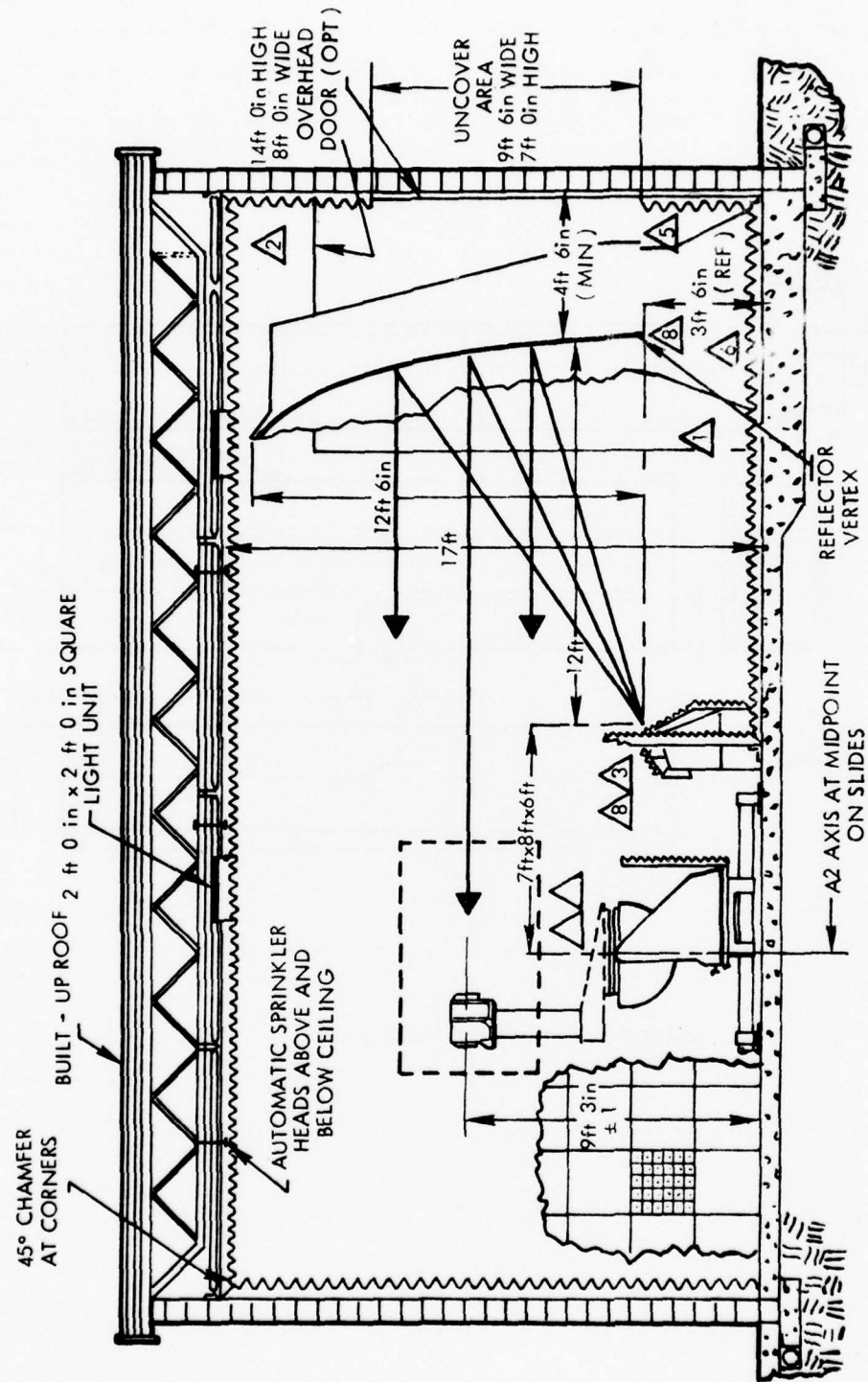


Figure 4 - Filter Retainer

UNCLASSIFIED



UNCLASSIFIED

Figure 5 - Raytheon Compact Range Facility

UNCLASSIFIED

TABLE 1
COMPACT RANGE PHYSICAL AND PERFORMANCE PARAMETERS

Overall Size	36 ft long x 20 ft wide x 16.5 ft high
Frequency Range	2.6 - 18 GHz
Antenna Size	4 ft diameter or less
Amplitude Taper	0.5 dB
Phase Variation	$\pm 5^\circ$
Reflector	
Type	Offset Parabola
Size	16 ft wide x 12 ft high (27 ft diameter)
F/D	0.6
Weight	5000 lbs
Surface Specification	± 0.002 (2 ft x 2 ft) ± 0.010 (overall)
Surface Actual	± 0.003 rms from ideal
Surface Type	Machined epoxy with silver film
Frame	Welded steel truss
Source	
Low Reradiation	Circular Horn
Low Back Radiation	Circular WG. chokes
Illumination	Equal Pattern Tapers
Taper	-2 dB at edge of reflector
Typical Performance	
X-band	8 - 12 GHz
Test Antenna Diameter	3 ft
Amplifier Taper	0.3 dB
Phase Taper	7.5°
Stray Radiation	-40 dB
Polarization Tilt	1° /ft.

UNCLASSIFIED

2.2 Analysis of Filter Configuration

The final design configuration for the experimental filter is shown in Figure 6 and will be discussed to provide a reference for the predicted and measured performance of the actual filter. TE and TM rejection characteristics are shown in Figures 7 and 8, respectively. In the passband, maximum reflection loss is less than 1 dB and occurs at 10° from broadside at 9.31 GHz in both planes. Over the remainder of the passband, and throughout the frequency band, reflection loss is less than 0.5 dB. The design shows a slight improvement for TM incidence over the initial design, (Reference 1) in that the onset of the stopband occurs inside 25° . However, this is at the expense of greater passband reflection loss and earlier onset of the Brewster angle passband (Reference 1). The ripple occurring in the stopband for both planes of incidence is due to the increased total filter thickness.

	t (in)
$\epsilon = 5.09$	0.468
$\epsilon = 1.02$	2.441
$\epsilon = 9.81$	0.266
$\epsilon = 1.02$	1.857
$\epsilon = 23.55$	0.153
$\epsilon = 1.02$	0.617
$\epsilon = 22.68$	0.200
$\epsilon = 1.02$	0.598
$\epsilon = 9.72$	0.246
$\epsilon = 1.02$	0.637
$\epsilon = 4.98$	0.088

Figure 6 - Final Design Configuration

UNCLASSIFIED

UNCLASSIFIED

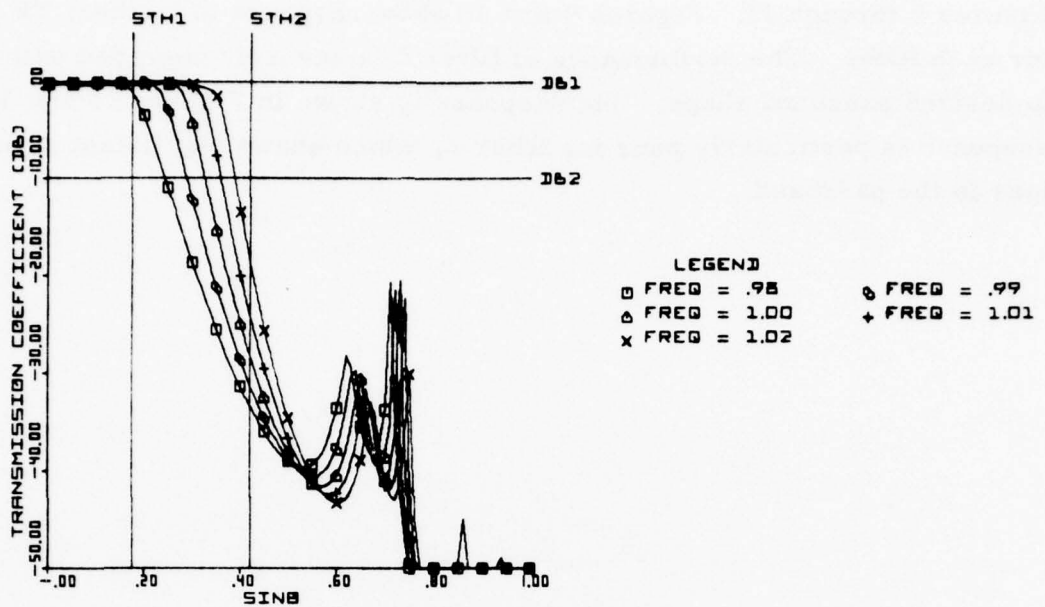


Figure 7 - TE Power Transmission Coefficient - Final Design Consideration

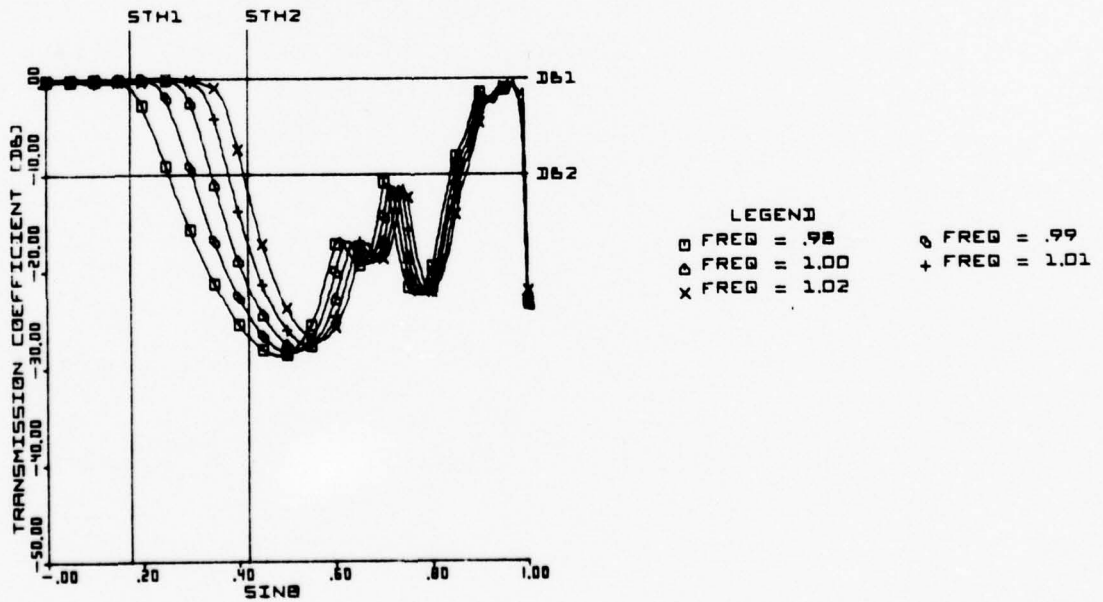


Figure 8 - TM Power Transmission Coefficient - Final Design Configuration

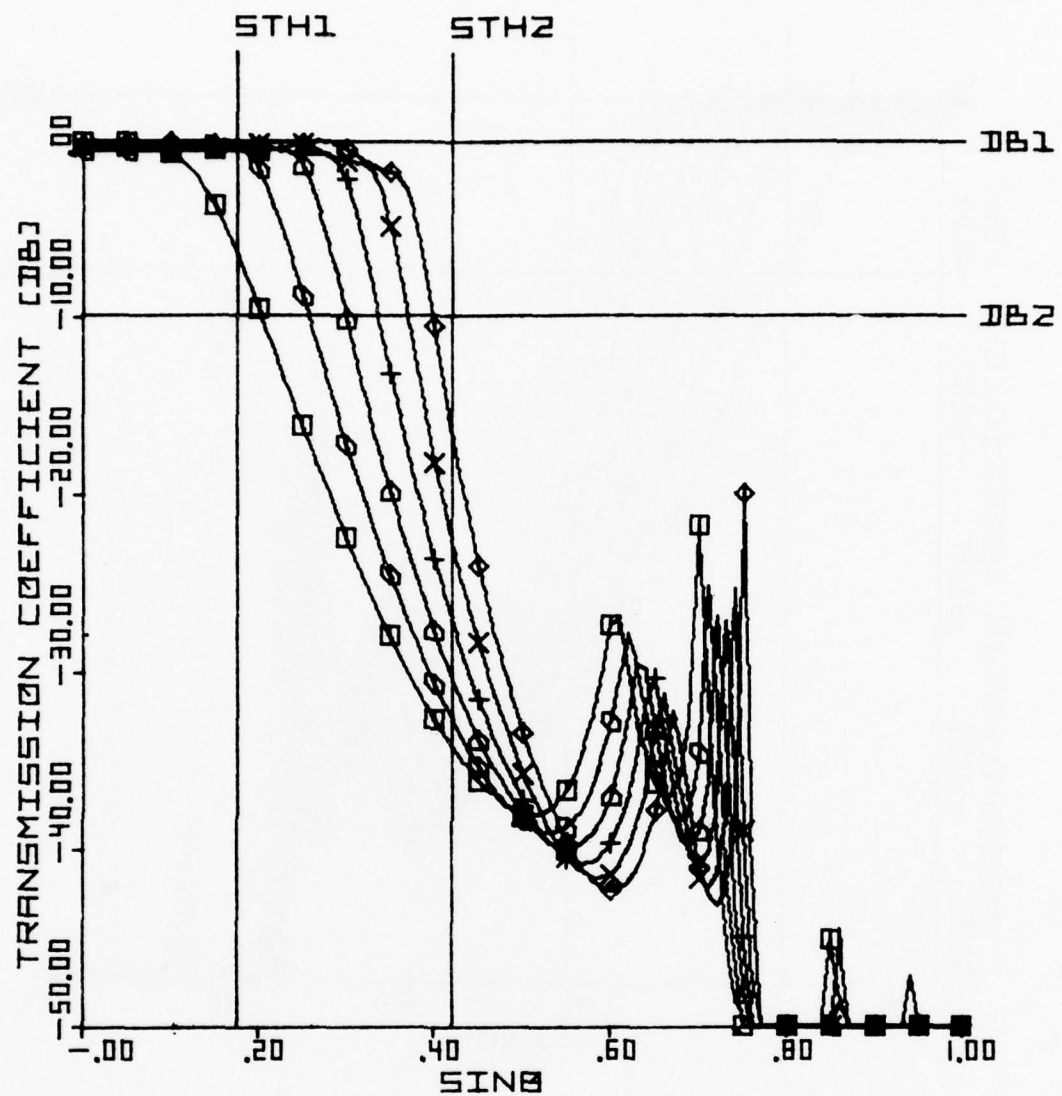
UNCLASSIFIED

UNCLASSIFIED

The predicted performance of the experimental filters* is shown in Figures 9 through 12. Figures 9 and 10 show response to incident TE waves for each filter. The performance of filter 2 is severely degraded with respect to desired passband shape. TM response is shown in Figures 11 and 12. TM response is particularly poor for filter 2, which shows significant reflection loss in the passband.

* Hereafter, the filter halves will be referred to as filter 1 and filter 2, as indicated in Figure 3.

UNCLASSIFIED



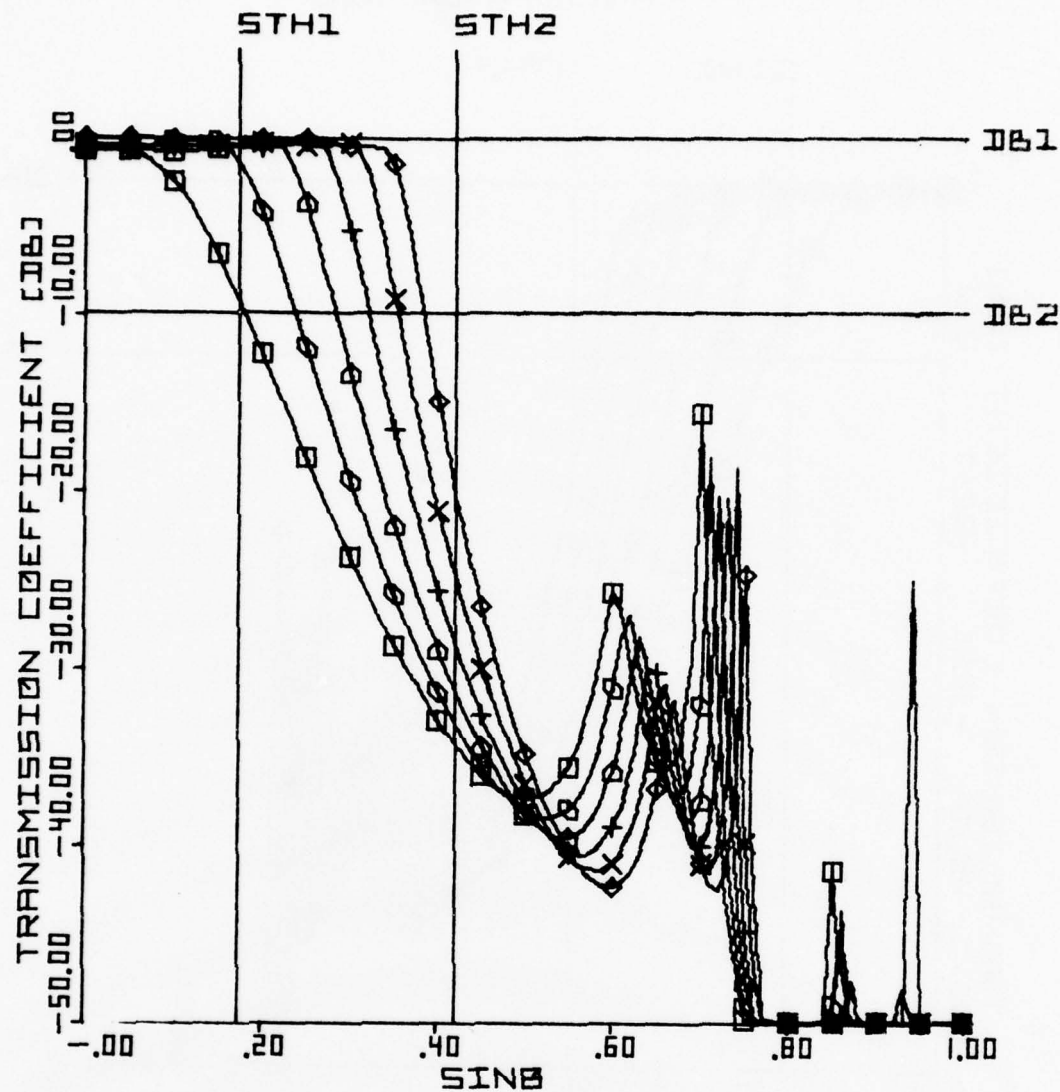
LEGEND

□ FREQ = .97	○ FREQ = .98
△ FREQ = .99	+ FREQ = 1.00
✗ FREQ = 1.01	◊ FREQ = 1.02

Figure 9 - TE Power Transmission Coefficient - Filter 1
($f_o = 9.5 \text{ GHz}$)
15

UNCLASSIFIED

UNCLASSIFIED



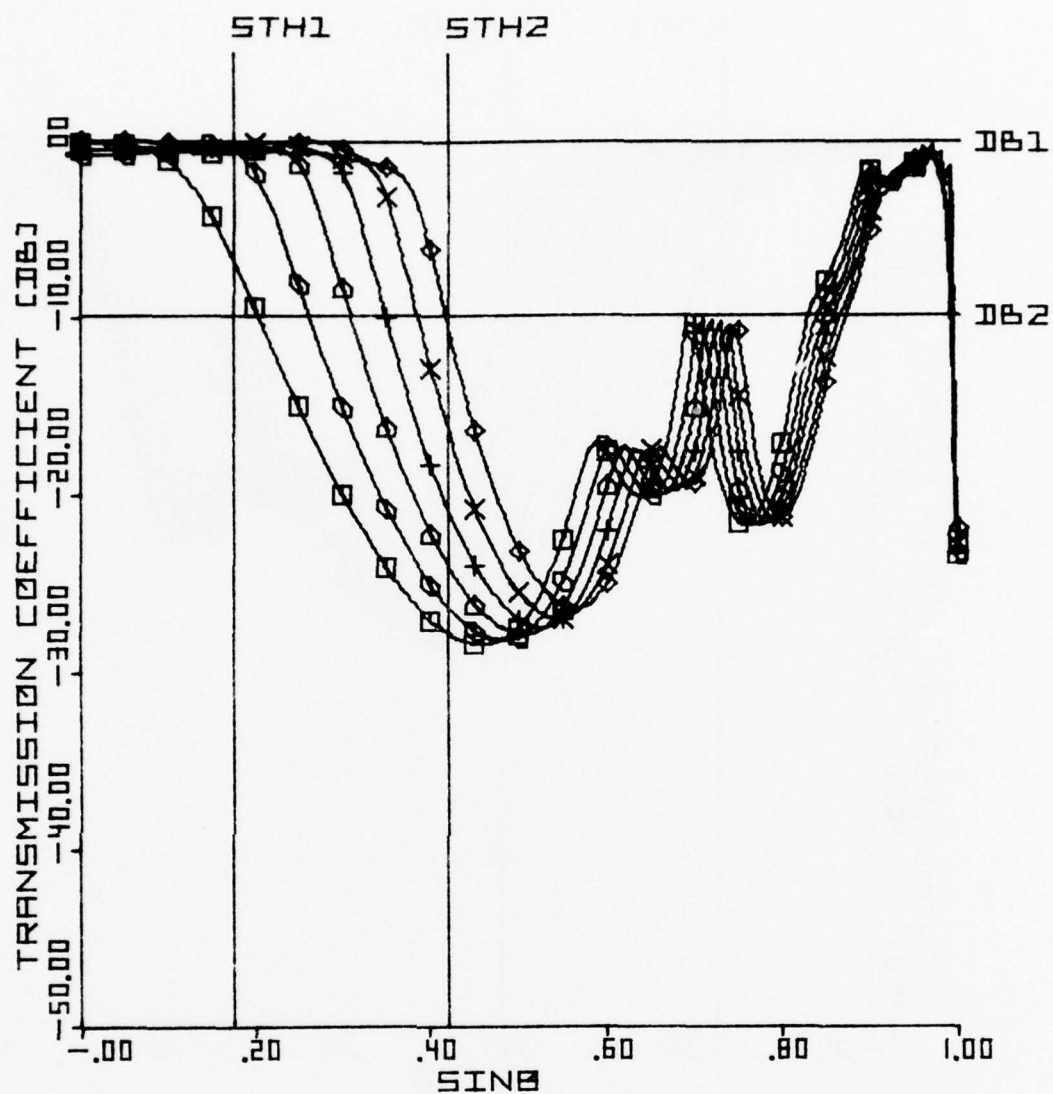
LEGEND

- | | |
|---------------|---------------|
| □ FREQ = .97 | ○ FREQ = .98 |
| △ FREQ = .99 | + FREQ = 1.00 |
| ✗ FREQ = 1.01 | ◊ FREQ = 1.02 |

Figure 10 - TE Power Transmission Coefficient - Filter 2
($f_o = 9.5$ GHz)

UNCLASSIFIED

UNCLASSIFIED



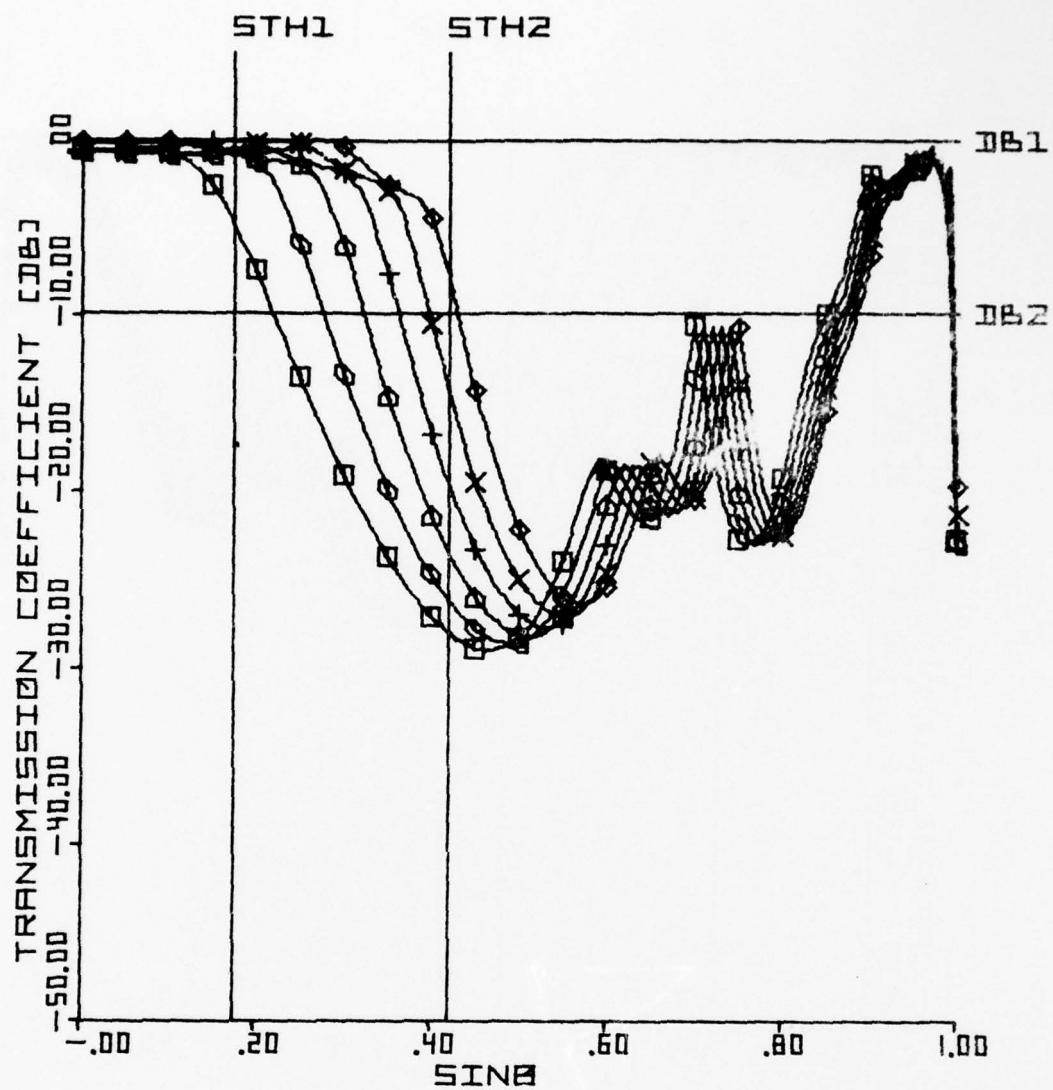
LEGEND

- | | |
|--------------|---------------|
| □ FREQ = .97 | ○ FREQ = .98 |
| △ FREQ = .99 | + FREQ = 1.00 |
| × | ◆ FREQ = 1.02 |

Figure 11 - TM Power Transmission Coefficient - Filter 1
($f_o = 9.5$ GHz)

UNCLASSIFIED

UNCLASSIFIED



LEGEND

- | | |
|--------------|---------------|
| □ FREQ = .97 | ○ FREQ = .98 |
| ◊ FREQ = .99 | + FREQ = 1.00 |
| × | × FREQ = 1.01 |
| | ◊ FREQ = 1.02 |

Figure 12 - TM Power Transmission Coefficient - Filter 2
($f_o = 9.5$ GHz)

UNCLASSIFIED

UNCLASSIFIED

2.3 Measured Filter Response to TE and TM Plane Waves

To determine transmission characteristics, the filters were independently studied using a rectangular waveguide probe butted against the filter. The probe studies resulted in direct measurement of relative filter transmission coefficient out to 90° for TM incidence and approximately 25° for TE incidence. Absolute transmission loss in the passband was measured in the range of 3 to 4 dB.

2.3.1 Measured Filter Transmission Loss

The mechanism responsible for the measured transmission loss is problematic. Two sources are immediately evident. The first is the probe mismatch induced by the filter. No effort was made to match the probe to either the free-space or filter environment. Consequently, the introduction of the filter into the measurement system has an equal chance of either improving the match at the probe feed or giving further degradation. The second source of transmission loss is the large depth-to-height aspect ratio of the filter which, in essence, clips the filter frontplane distribution required for normal filter response. Based on some simple physical arguments it is reasonable to assign to the bulk of the transmission loss to the first source.

Let $\epsilon_\rho(\underline{u})$ and $\epsilon_\psi(\underline{u})$ be the tangential cylindrical fourier transform components of the probe and flange. Without detailed knowledge of these components, it can still be shown that the admittance looking out of the probe reference to the dominant guide mode has the general form*

$$Y_{ap} = \iint_{-\infty}^{\infty} \left[Y^{TM}(\underline{u}) |\epsilon_\rho(\underline{u})|^2 + Y^{TE}(\underline{u}) |\epsilon_\psi(\underline{u})|^2 \right] d\underline{u} \quad (1)$$

where $Y^{TM}(\underline{u})$ and $Y^{TE}(\underline{u})$ are the TE and TM admittances just outside the probe, looking away from the aperture, and \underline{u} is the free space transverse wavenumber integration variable. It is evident from Equation (1) that both the real and imaginary parts (conductance and susceptance) are significantly altered by the introduction of the spatial filter close to the probe. In particular,

* See, for instance, Reference 4.

UNCLASSIFIED

for any direction (\underline{u}), in or outside visible space ($|\underline{u}| \leq k$ or $|\underline{u}| > k$, respectively), $Y^{TM}(\underline{u})$ and $Y^{TE}(\underline{u})$ are simply the magnetic fields at the aperture plane for unit electric fields incident on the filter back face in the direction \underline{u} , and therefore are directly related to the filter planewave transmission properties. Hence, the angular filter response significantly alters the aperture admittance, and, consequently match at the probe exciter. A similar argument applies to filter interaction with infinite arrays of identical radiators and is treated more fully in Appendix B.

To evaluate the possible effects of filter cross-section aspect ratio on passband power loss, it is instructive to consider a simple two-dimensional configuration, as shown in Figure 13. Let it be assumed that the transmission response of a hypothetical spatial filter is a spatial pulse function, as shown

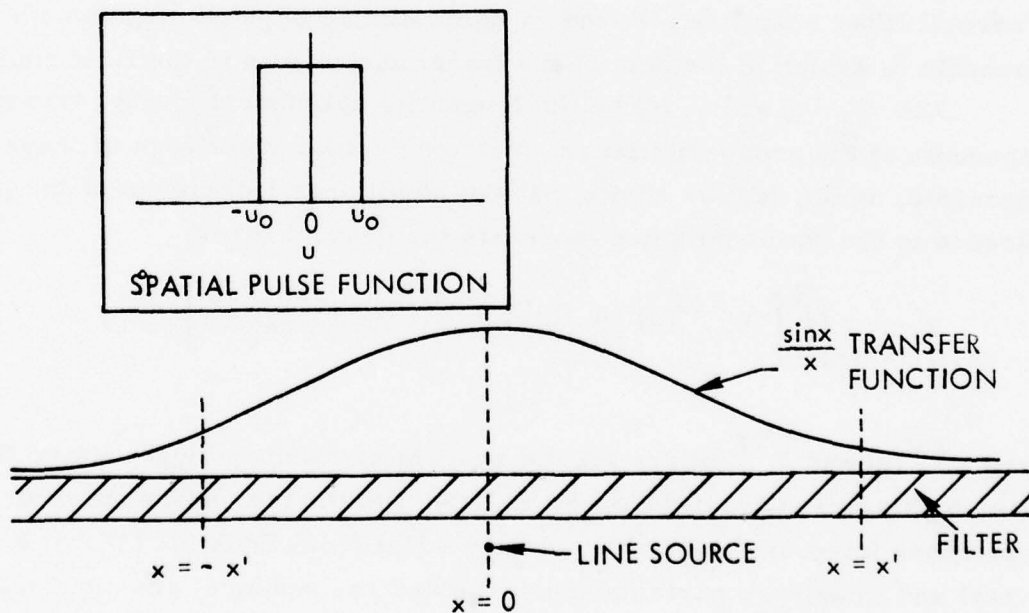


Figure 13 - Spatial Pulse Function Generator

UNCLASSIFIED

in the inset, where the pulse width is twice the passband width (u_0) in wavenumber space. If, on transmit, the wavenumber generator at the filter back-face gives a uniform distribution (i.e., is a line source perpendicular to the representation in the figure), then the transfer function to a point, x , on the front face of the filter must be given as

$$T(x)|_{z=h} = A \frac{\sin u_0 x}{u_0 x}, \quad -\infty < x < \infty \quad (2)$$

Where A is an appropriately chosen normalization. If, now, A is held constant (that is, the source current is constant), and the domain of x is limited to $-x' \leq x \leq x'$ by placing perfect absorber symmetrically about $x = 0$ in the $z = h$ plane, the properly normalized far electric field is

$$F(x', u_0, u) = \left\{ \frac{1}{\pi} \operatorname{Si}[x'(u_0 - u)] + \operatorname{Si}[x'(u_0 + u)] \right\} \quad (3)$$

where u is an arbitrary direction in wavenumber space, and $\operatorname{Si}(\xi)$ is the sine integral, given as

$$\operatorname{Si}(\xi) = \int_0^\xi \frac{\sin t}{t} dt \quad (4)$$

Figure 14 shows $F(x', u_0, 0)$ versus $2x'/\lambda$ for $u_0 = (2\pi/\lambda) \sin 10^\circ$. From the figure, it is clear that significant broadside power loss occurs for

$2x'/\lambda < 3.46$ or at 9.5 GHz,
 $2x' < 4.29$ in. Consequently for the unobstructed/aperture of the experimental filter, it is concluded that transmission loss in the passband due to aspect ratio is potentially insignificant with respect to loss due to aperture mismatch.

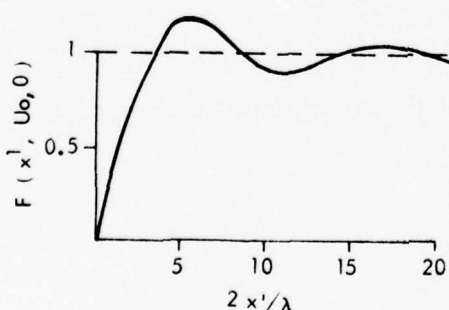


Figure 14 - $F(x', u_0, 0)$ versus $2x'/\lambda$ for 10° Passband

UNCLASSIFIED

UNCLASSIFIED

2.3.2 Measured Relative Response

Measured filter response was determined with the probe electric field perpendicular to the filter long dimension (TE incidence) and parallel to the filter long dimension (TM incidence). For TE incidence, the probe pattern modifies the filter response beyond approximately 25° from broadside - hence, beyond, the measured results can not be interpreted as a direct measure of filter properties. For TM incidence, the probe may be assumed to radiate uniformly.

For TE incidence (H-plane with respect to the probe), the shape of the passband and filter skirts are in good agreement with predicted data for the actual filter, as shown in Figure 15 for Filter-1 at 9.41 GHz. However, throughout the remainder of the stopband, the sidelobes are significantly greater than might be expected. This behavior can be explained by again considering the effect of truncating the distribution required to obtain a spatial pulse function from a line source. Examination of Equation (3) shows that for $|u| > |u_0|$, significant cancellation of the sine integrals is obtained. However, for finite aperture size, this cancellation is not complete and a complex side-lobe structure is obtained in the stopband. Typical sidelobe structure for a $\sin x/x$ distribution truncated at $\pm 10\lambda$ is shown in Figure 16. The discontinuities in the pattern are due to the sampling interval.

Figure 17 shows measured and predicted performance of Filter-1 for TM incidence at 9.41 GHz. Again, the principal features of the spatial passband are obtained without significant distortion. Also, the properties of the spurious passband are well defined. The excessive ripple in the stopband is clearly associated with the truncation of the filter.

Figures 18 and 19 show TE and TM filter response for Filter-1. The principal pattern variation with frequency is clearly evident. An increase in frequency results in an increase in width of the spatial passband for both polarizations.

UNCLASSIFIED

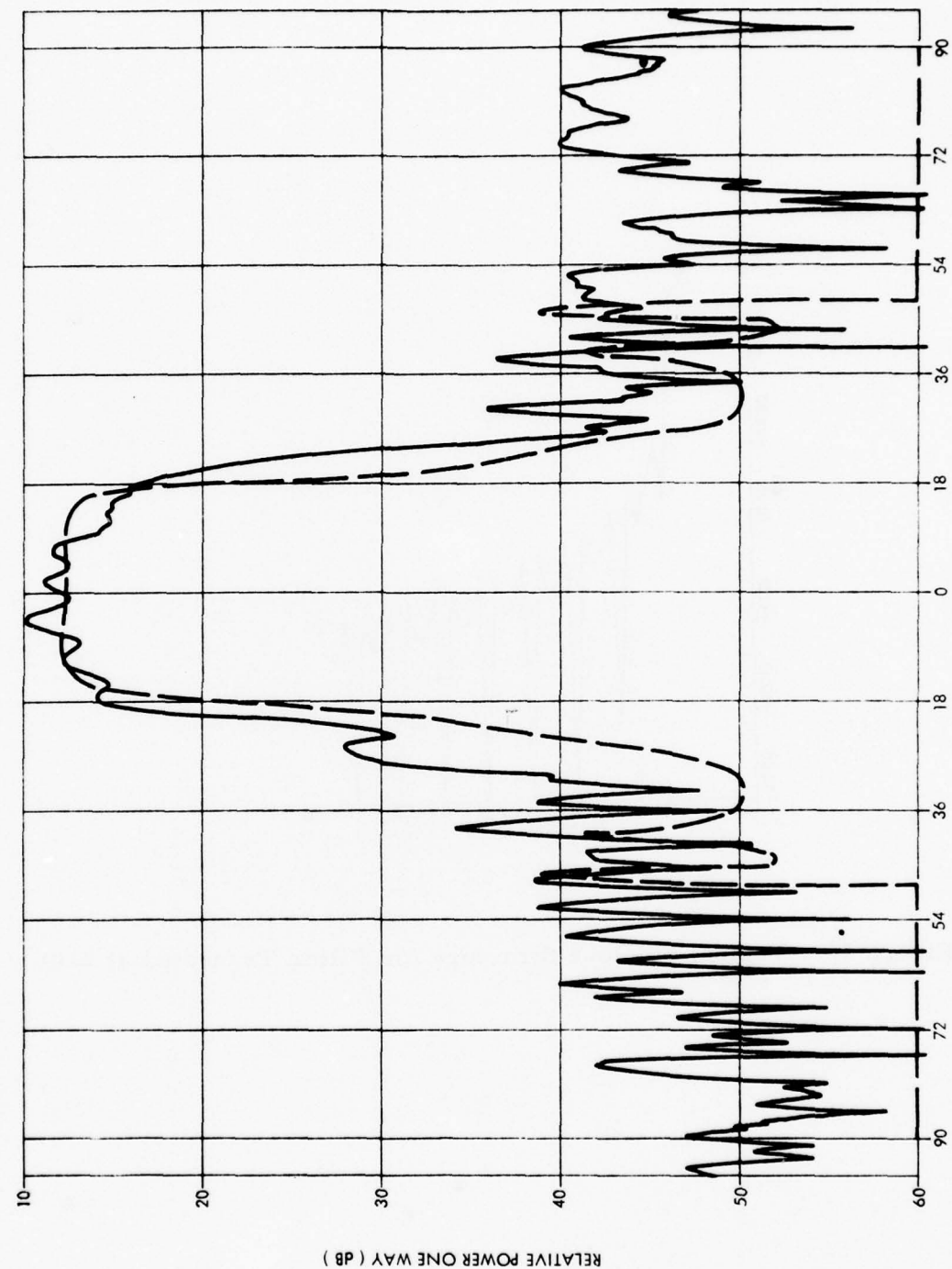


Figure 15 - Filter-1 TE Response - 9, 41 GHz

UNCLASSIFIED

UNCLASSIFIED

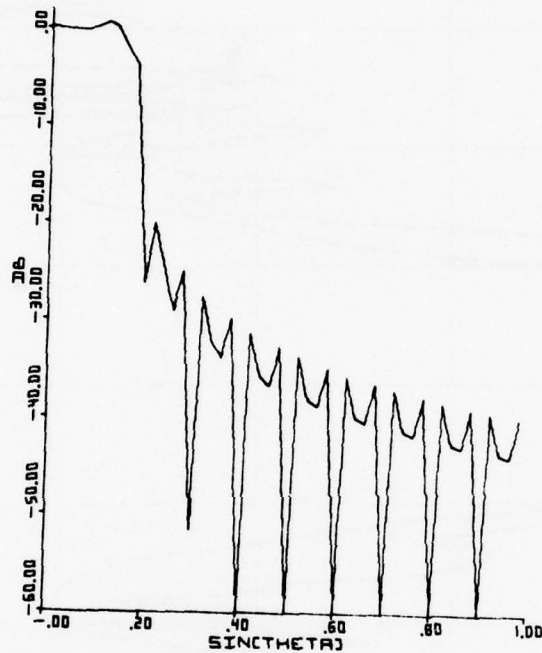


Figure 16 - Typical Sidelobe Structure for Filter Truncated at $\pm 10\lambda$

UNCLASSIFIED

UNCLASSIFIED

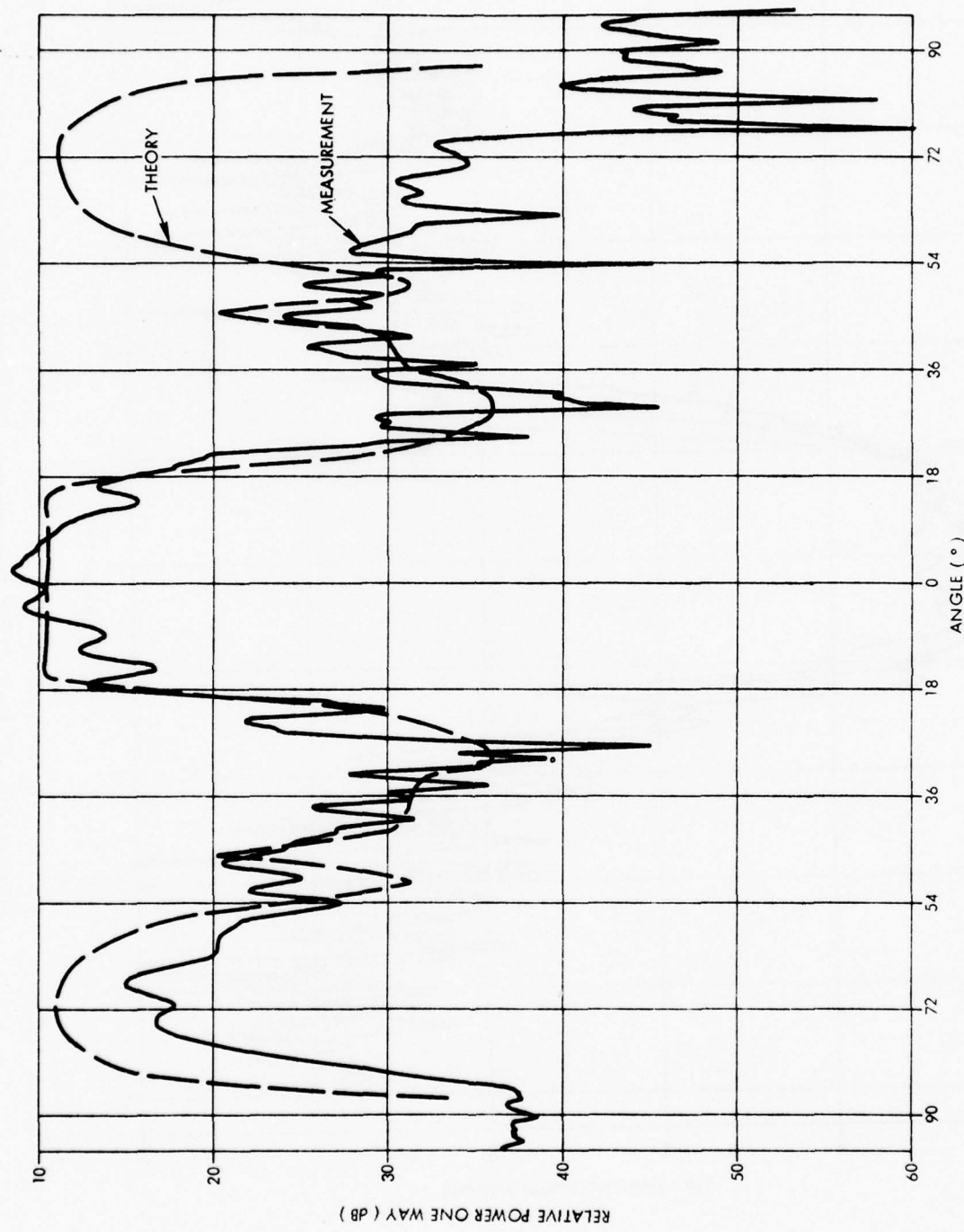


Figure 17 - Filter-1 TM Response -9. 41 GHz

UNCLASSIFIED

UNCLASSIFIED

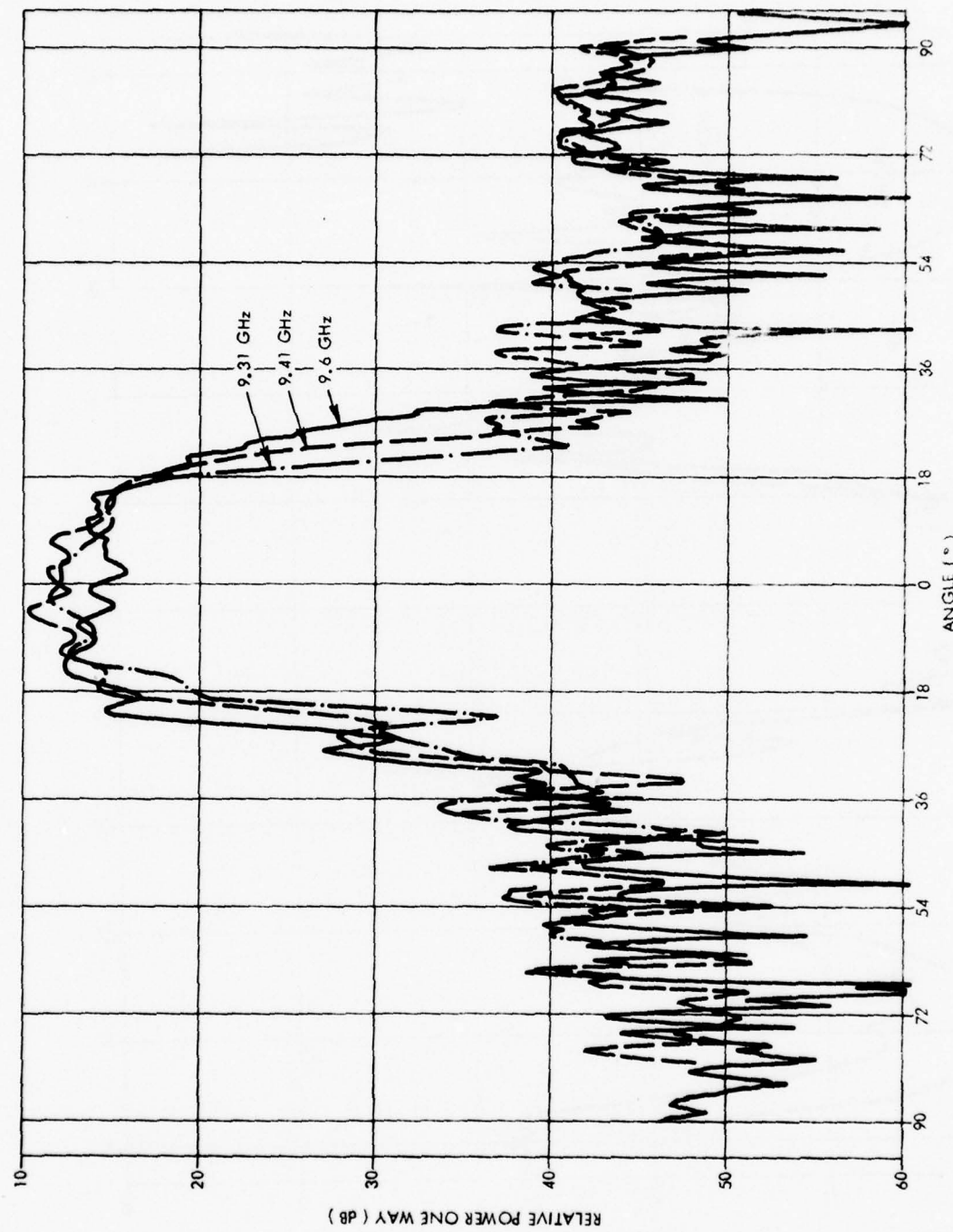


Figure 18 - Filter-1 TE Response - Parameter Frequency

UNCLASSIFIED

UNCLASSIFIED

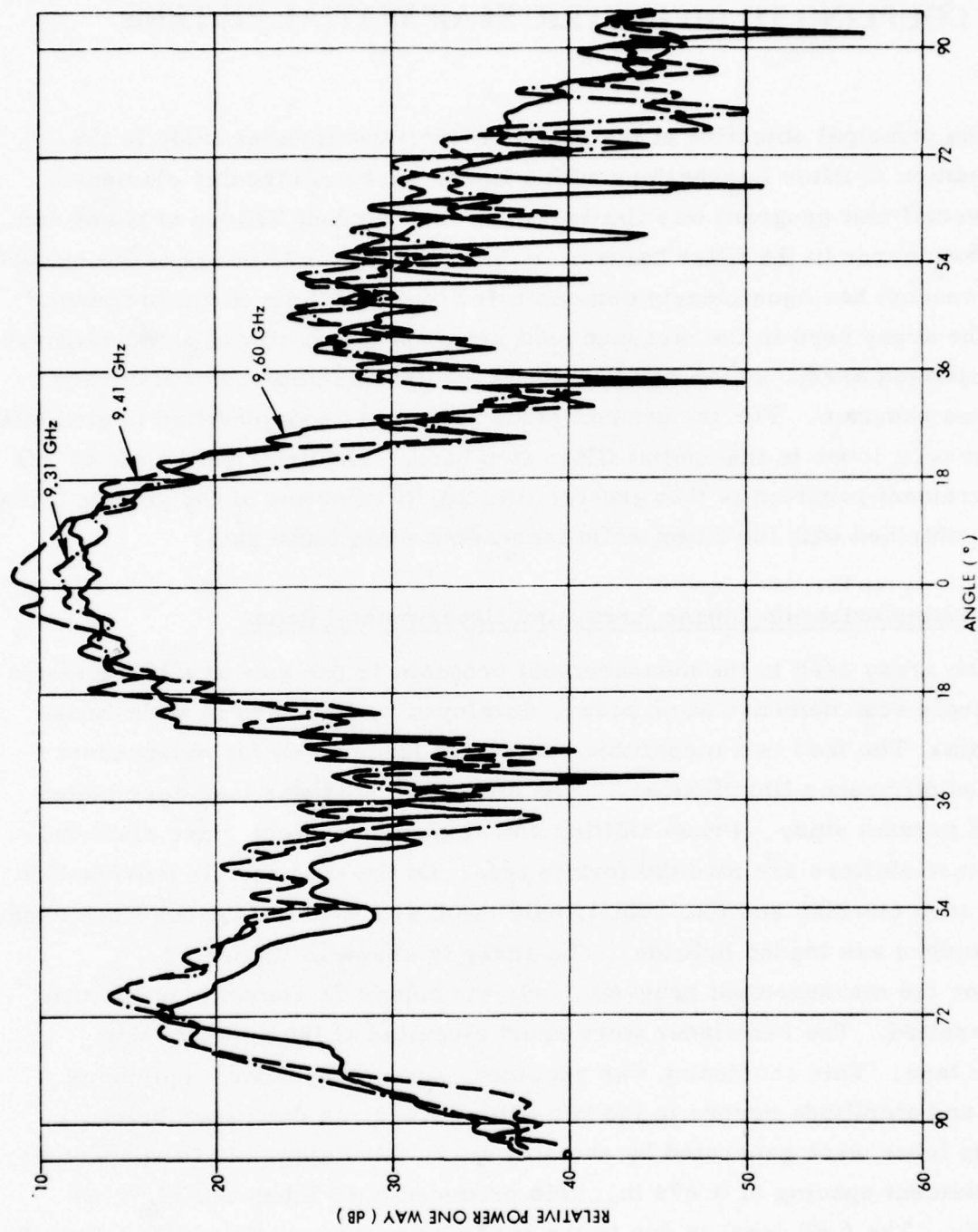


Figure 19 - Filter-1 TM Response - Parameter Frequency

UNCLASSIFIED

UNCLASSIFIED

III. EXPERIMENTAL INVESTIGATION OF LINEAR ARRAY COUPLING TO DIELECTRIC SLAB SPATIAL FILTERS

The principal objective of the spatial filter experimental study is the examination of filter interactions with a linear array of circular elements. The overall test program was limited by the independent buildup of phase and amplitude error in the filter halves. However, the effectiveness of the spatial filter concept has been clearly demonstrated by the measurement program.

The array used in the measurement program is one row of a 128-element linear phased array, which was developed for demonstration in a Raytheon in-house program. For the present study, the array was modified to generate 6 dB grating lobes in the spatial filter stop band. The principal result of this measurement program is that greater than 23 dB rejection of the grating lobes can be obtained with the filter while increasing main beam gain.

3.1 Multipolarization Linear Array and Experimental Setup

The array used in the measurement program is one row of a 128-element wide angle scan demonstration array, developed by Raytheon in an in-house program. The feed is a monolithic center-fed ladder feed for independent sum and difference illuminations. The difference port was load-terminated for the present study. Phase shifting and amplitude switching are electronic. The phase shifters are toroidal ferrite type. Of the six possible polarization states (two circular and four lines), only the E and H-polarizations were used. All couplers are loaded hybrids. The array is shown in Figure 20.

For the measurement program, only the center 32 elements of the row were excited. The remainder were short circuited at the aperture with copper tape. This shortening was required, due to independent buildup of phase and amplitude errors in the two filter halves, as discussed below. Grating lobes were generated by shorting every third element at the aperture. With element spacing of 0.674 in., this produced 6 dB lobes at $\pm 37.9^\circ$ at 9.5 GHz. The 6 dB level is due to the subarray pattern of the excited element pairs.

UNCLASSIFIED

UNCLASSIFIED

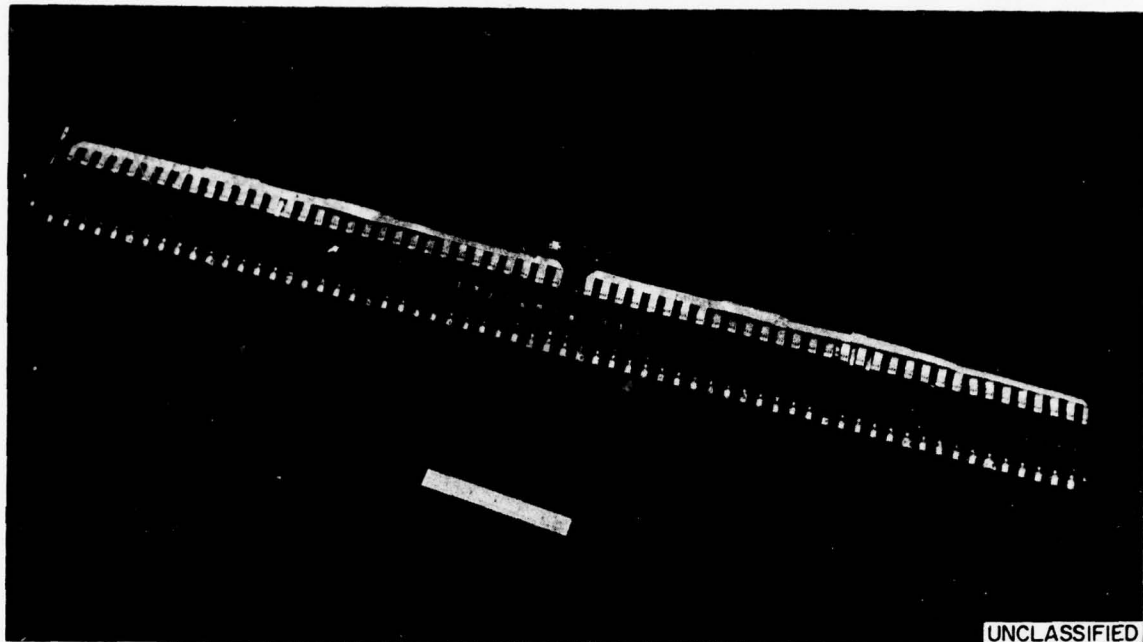


Figure 20 - 128-Element Multiple Polarization Linear Array CN-6-1932

The array/filter mount is shown in Figure 21. The mount is constructed of plywood. The alignment holes shown in the figure were to provide accurate tilt of the array, with respect to the filter normal. Due to the independent phase and amplitude errors on the filter halves, it was necessary to translate both filter and array, such that the array center was alternately aligned with the centers of each filter half. In this manner, patterns were measured on each filter half independently.

For the array/filter measurements, free space absorbers were configured to enclose the array and filter backface and edges.

The measurement program was conducted at the Raytheon Compact Range Facility described in Subsection 2.1.

UNCLASSIFIED

UNCLASSIFIED

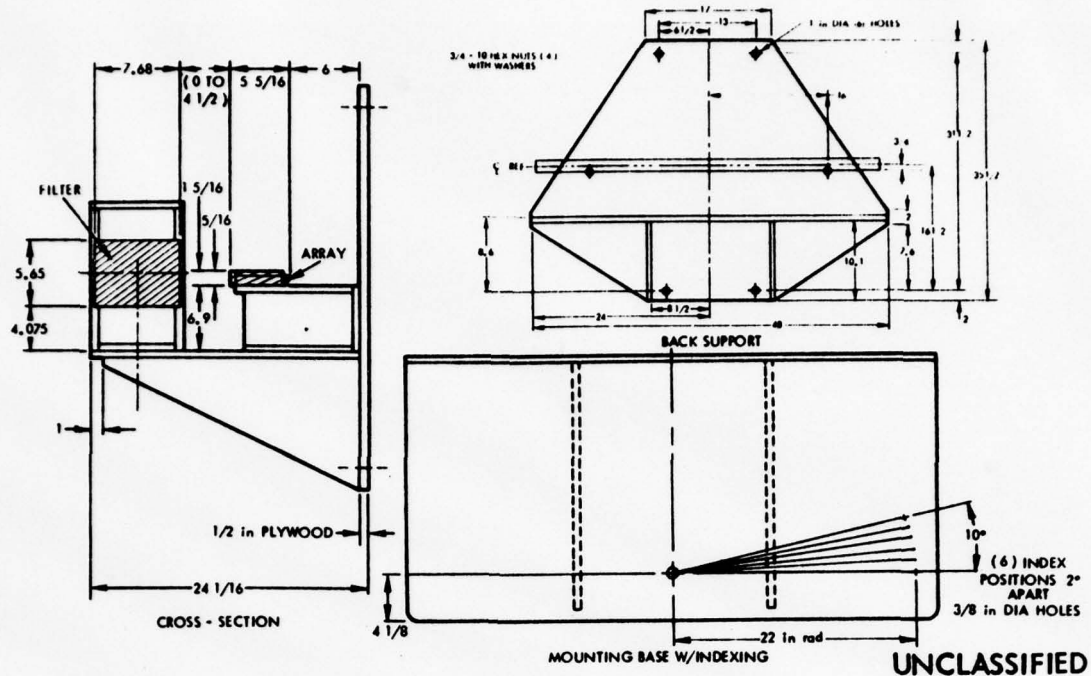


Figure 21 - Array/Filter Mount

3.2 Pattern Measurement Program

Initially, pattern properties were studied using the full 64-element aperture and full filter length. These studies led to the necessity to independently characterize the filter halves, as described in Section 2, using a small waveguide probe. Figure 22 shows the result of these early measurements. Shown in the figure is a comparison of H-plane array patterns with and without the full-length filter. With the filter in place, there is a limited decrease in far-out sidelobes, and a significant increase and asymmetric structure to sidelobes in the passband. These properties arise primarily due to an imbalance in transmission phase, as seen by the following argument.

UNCLASSIFIED

UNCLASSIFIED

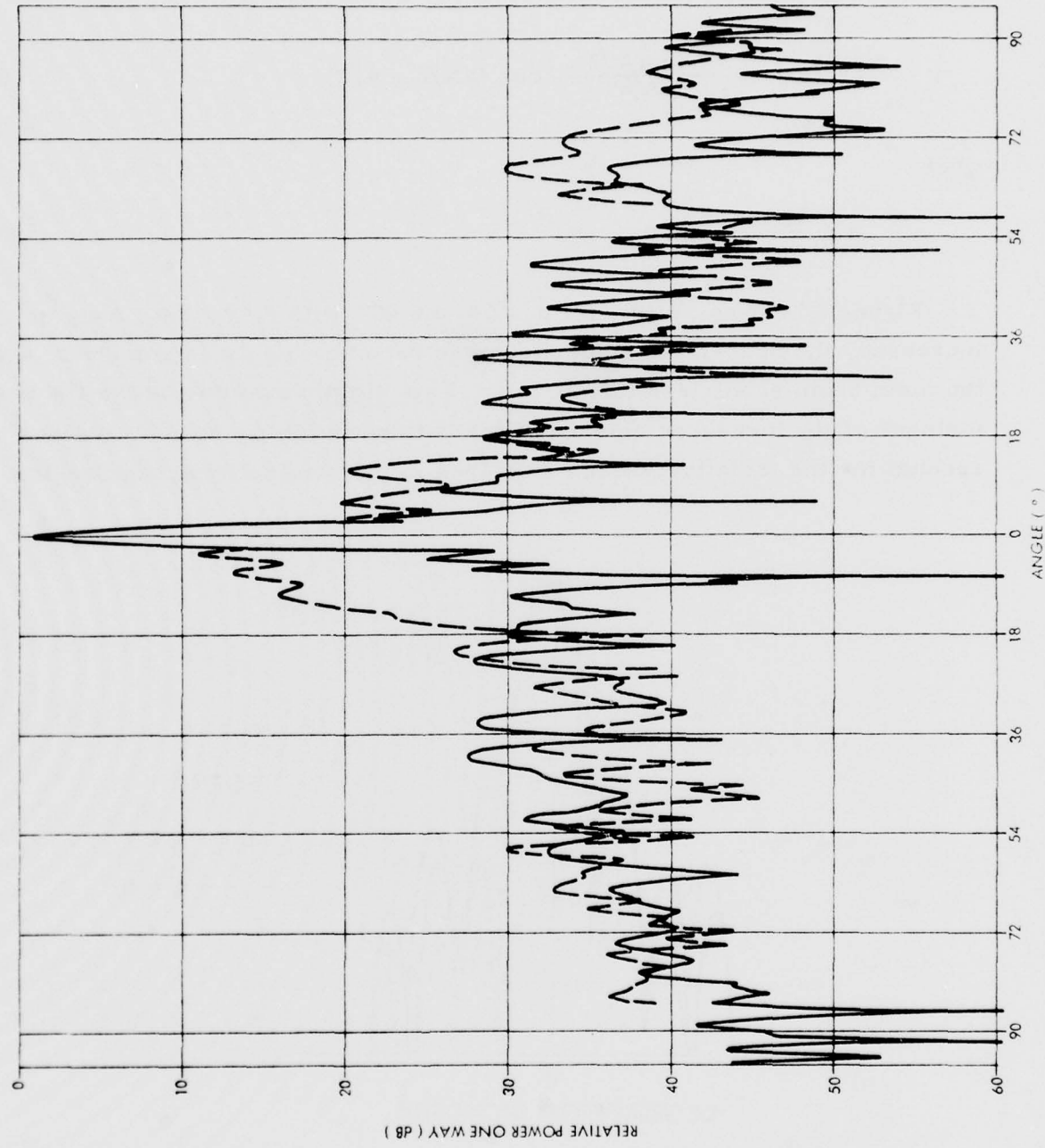


Figure 22 - Effect of Independent Phase and Amplitude Error Buildup - Full Filter - Full Array - 9.5 GHz

UNCLASSIFIED

UNCLASSIFIED

Let a pair of equal length and amplitude colinear, contiguous line sources of length A be out of phase by ϕ degrees. Then the normalized far-field magnitude is:

$$|E(\theta)| = \frac{\sin \mu A/2}{\mu A/2} \cos (\mu A/2 - \phi/2) \quad (5)$$

where

$$\mu = \frac{2\pi}{\lambda} \sin \theta \quad (6)$$

Figure 23 shows $|E(\theta)|$ for $\phi = 0^\circ$ and 40° with $A/\lambda = 24$. As ϕ is increased, the near-in sidelobe structure becomes highly asymmetric, while the main beam scans less than 0.25° . This simple example shows the basic features of the measured antenna/filter pattern in the passband, but does not account for the (relatively) high sidelobes in the nominal stop band region.

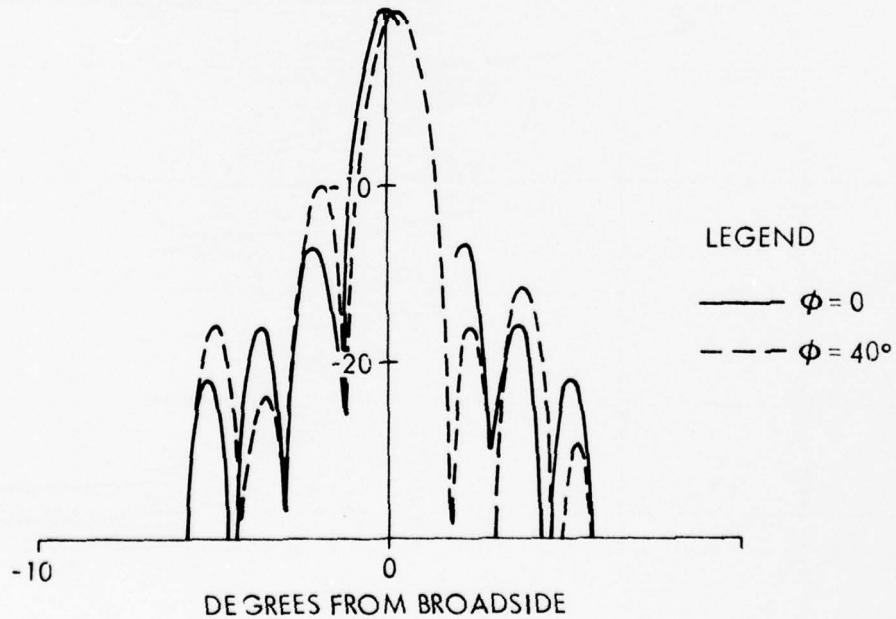


Figure 23 - Effects of Independent Phase Error - Line Source Model

UNCLASSIFIED

UNCLASSIFIED

This region can be explained, in part, by assuming the total filter imparts a $\sin(x)/x$ weighting to the effective element pattern, but with a phase discontinuity at the center of the filter. With this assumption, the filter transmission properties of a 20λ filter are shown in Figure 24 for three relative phases ($\phi = 0, 20, 40^\circ$). As the phase error increases, there is a dramatic decrease in stop band rejection (which is independent of total filter length).

Evidently, these simple arguments are not sufficient to completely explain the measured data, but are certainly primary contributors. The phase errors used in this illustration are typical of the actual buildup in the filter halves, due to dielectric constant error only.

Figure 25 shows a comparison of array patterns with and without filtering for the modified (short) array supporting grating lobes. For this particular measurement, the filter backplane and array are not enclosed by the absorber. The measurement is at 9.5 GHz using Filter 1. The principal result here is a 23 dB rejection of the grating lobes with simultaneous 3 dB increase in main beam gain. With Filter 1 in place, there is a slight deformation of the main beam and sidelobes in the passband are increased. Away from the grating lobes, sidelobe improvement is roughly 10-15 dB, indicating significant contribution due to secondary sources.

The increase in main beam gain is due to the reactive termination of the grating lobes by the filter. Since for an infinite array, all energy must appear at the feed port or one of the beam ports, the reactive termination of the grating lobes must result in an alteration of aperture fields, and hence, alter the array match. Specifically, since the beams are propagating in free space, the reflected energy will phase in and out at the feed port as the separation between array and filter is varied. Consequently, depending on array/filter spacing, the presence of the filter may improve the array match, as in the figure. In this measurement, and those to be discussed below, the array/filter spacing is 0.500 in. A more extensive treatment of filter/array coupling is given in Appendix B.

UNCLASSIFIED

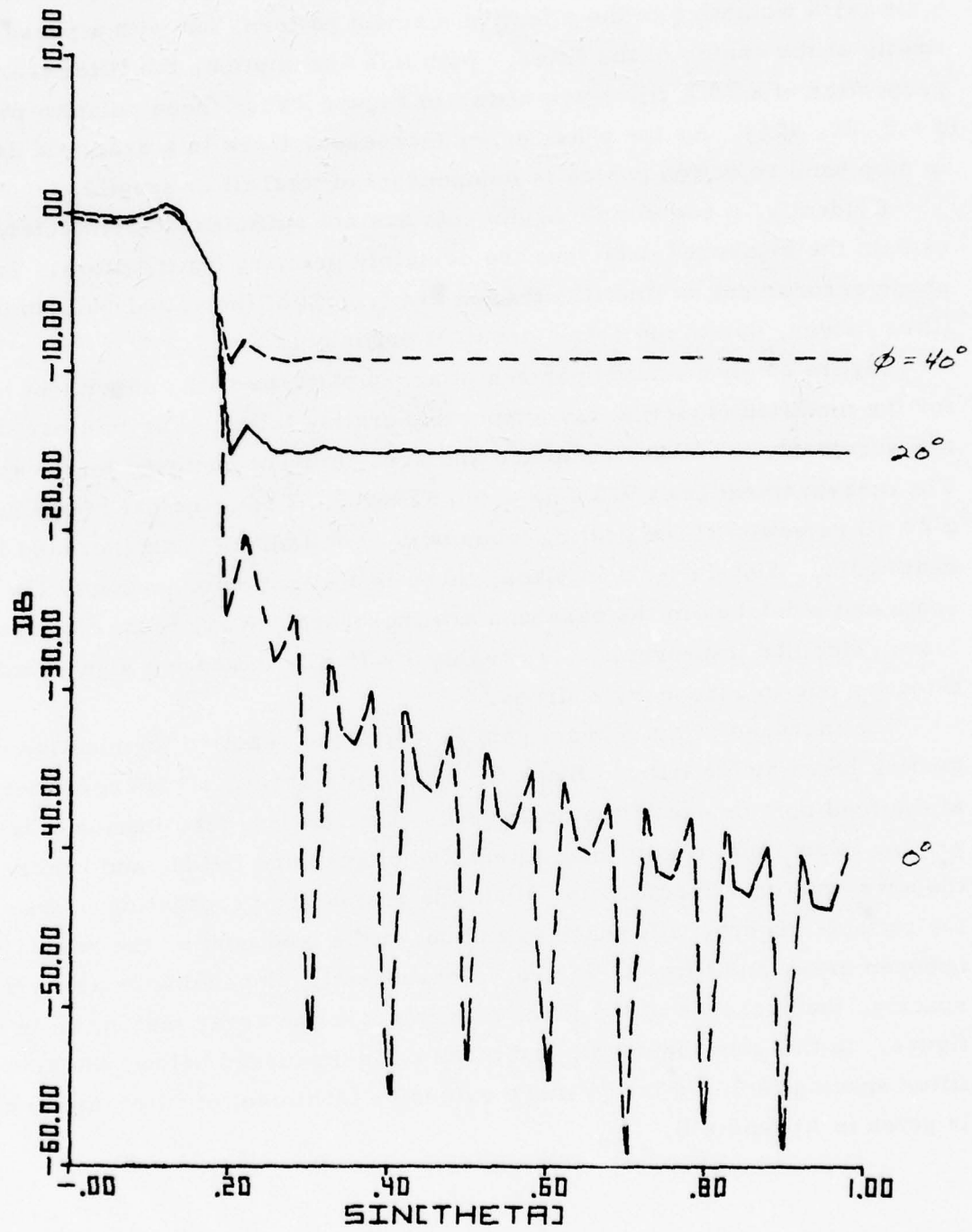


Figure 24 - Pattern Properties of 20λ Spatial Pulse Generator With Assumed Phase Error

UNCLASSIFIED

UNCLASSIFIED

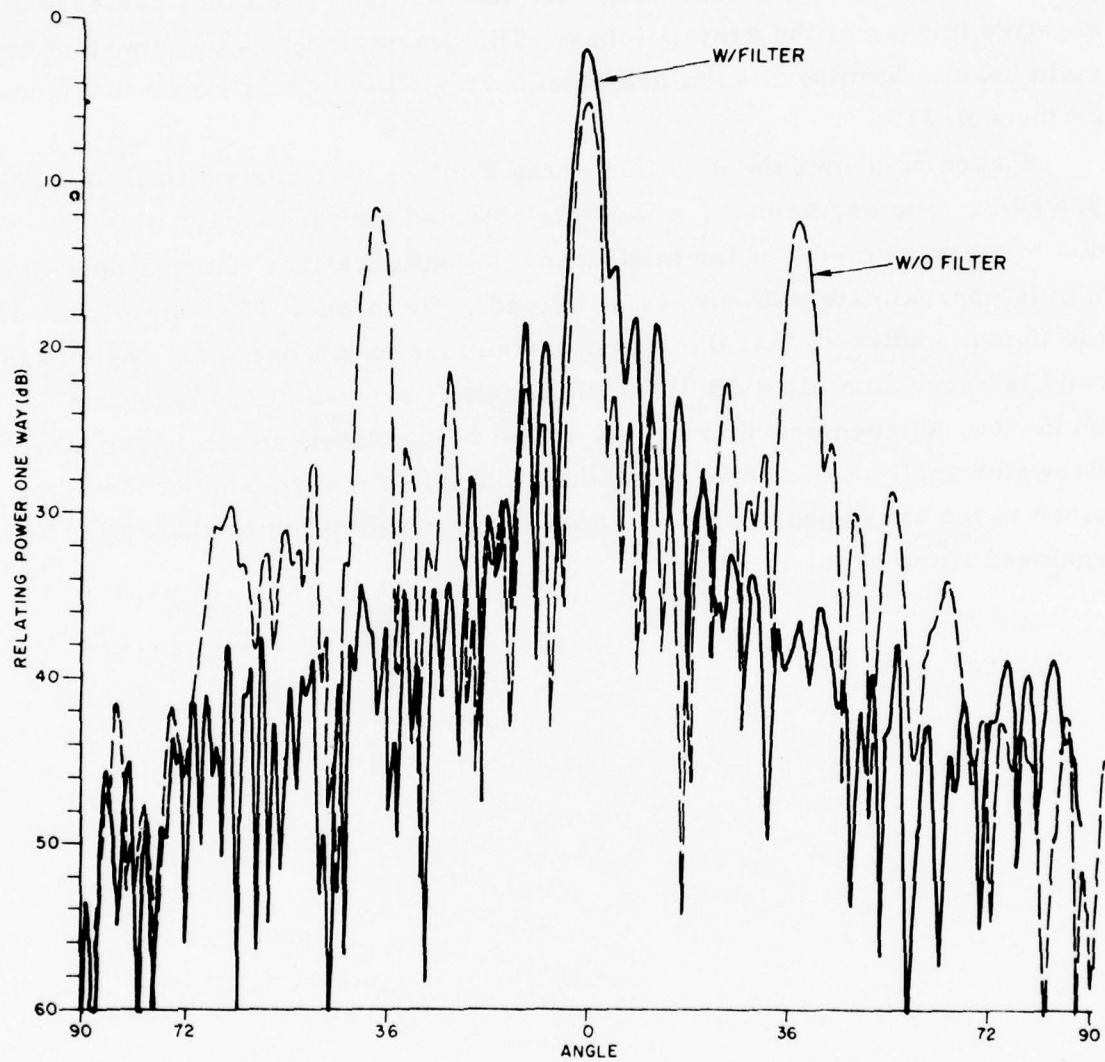


Figure 25 - H-Plane Modified Linear Array Pattern With and Without
Filter 1, 9.5 GHz

UNCLASSIFIED

UNCLASSIFIED

Figures 26 through 28 show modified array H-plane patterns with Filter 1, at 9.33, 9.5 and 9.69 GHz, respectively. For these and the following measurements, the filter backplane and array are enclosed in the absorber. The grating lobe rejection exceeds 28 dB at all frequencies. The heavily excited lobes at $\pm 144^\circ$ correspond to energy passing through the absorber enclosure and reflecting back into the feed port; they are essentially negative images of the grating lobes. The peak at 180° is the image of the main beam. Similar results are obtained for Filter 2, as shown in Figures 29 through 31.

Figure 32 shows the modified array E-plane patterns with Filter 1 at 9.5 GHz. The asymmetry, which was obtained for all E-plane patterns, is due to the asymmetry of the measurement configuration. Grating lobe rejection is approximately 22 dB, as predicted. The peak at 68° , on the left of the figure, indicates that the transmission loss in the Brewster angle passband is approximately 4 dB. The rapid falloff beyond 70° is typical of TM incidence, as seen previously. As shown by the insets in the figure, the Brewster angle passband is eliminated when the forward edge of the filter is close to the array phase center. This is most likely due to absorption at the enclosed filter edge.

UNCLASSIFIED

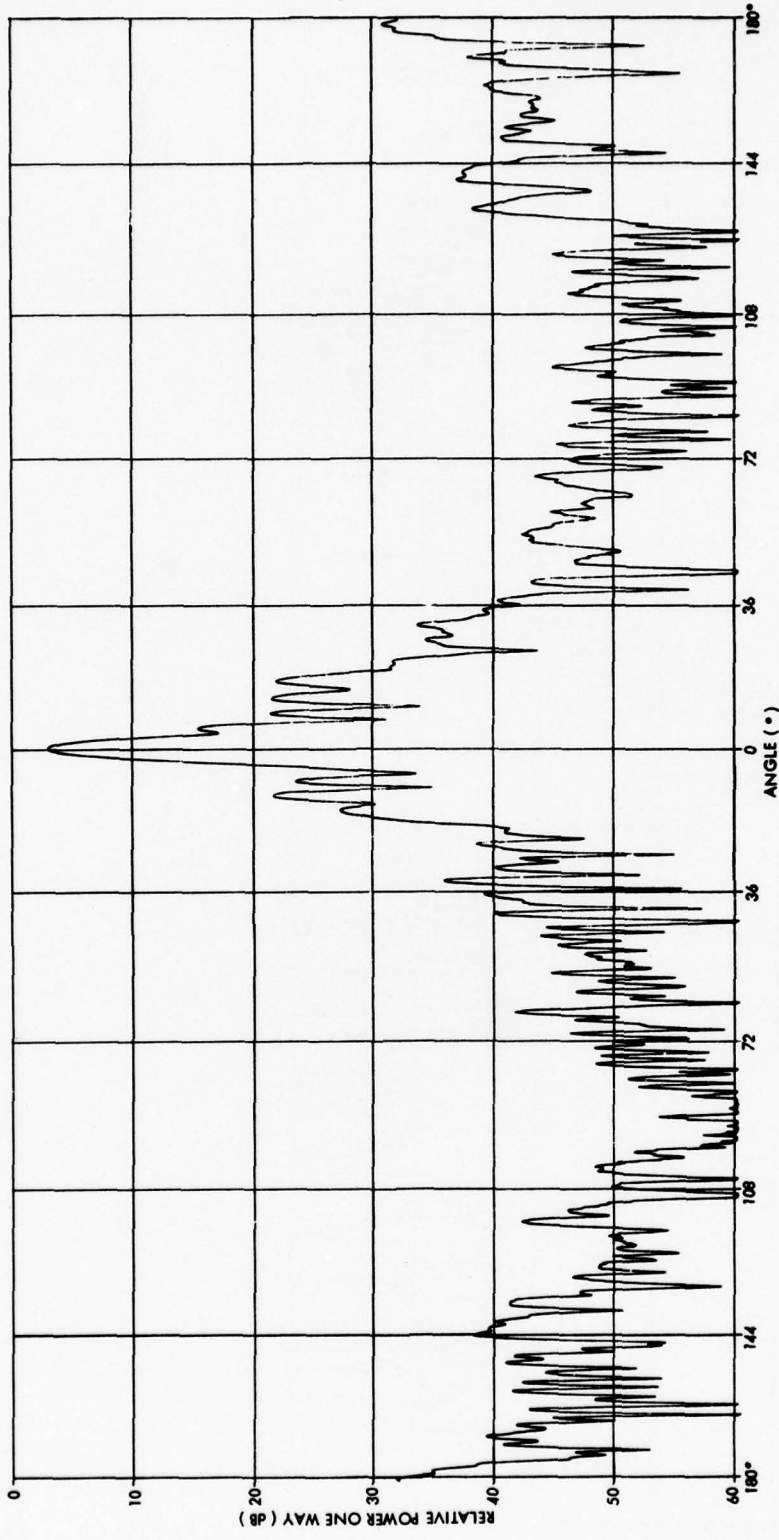
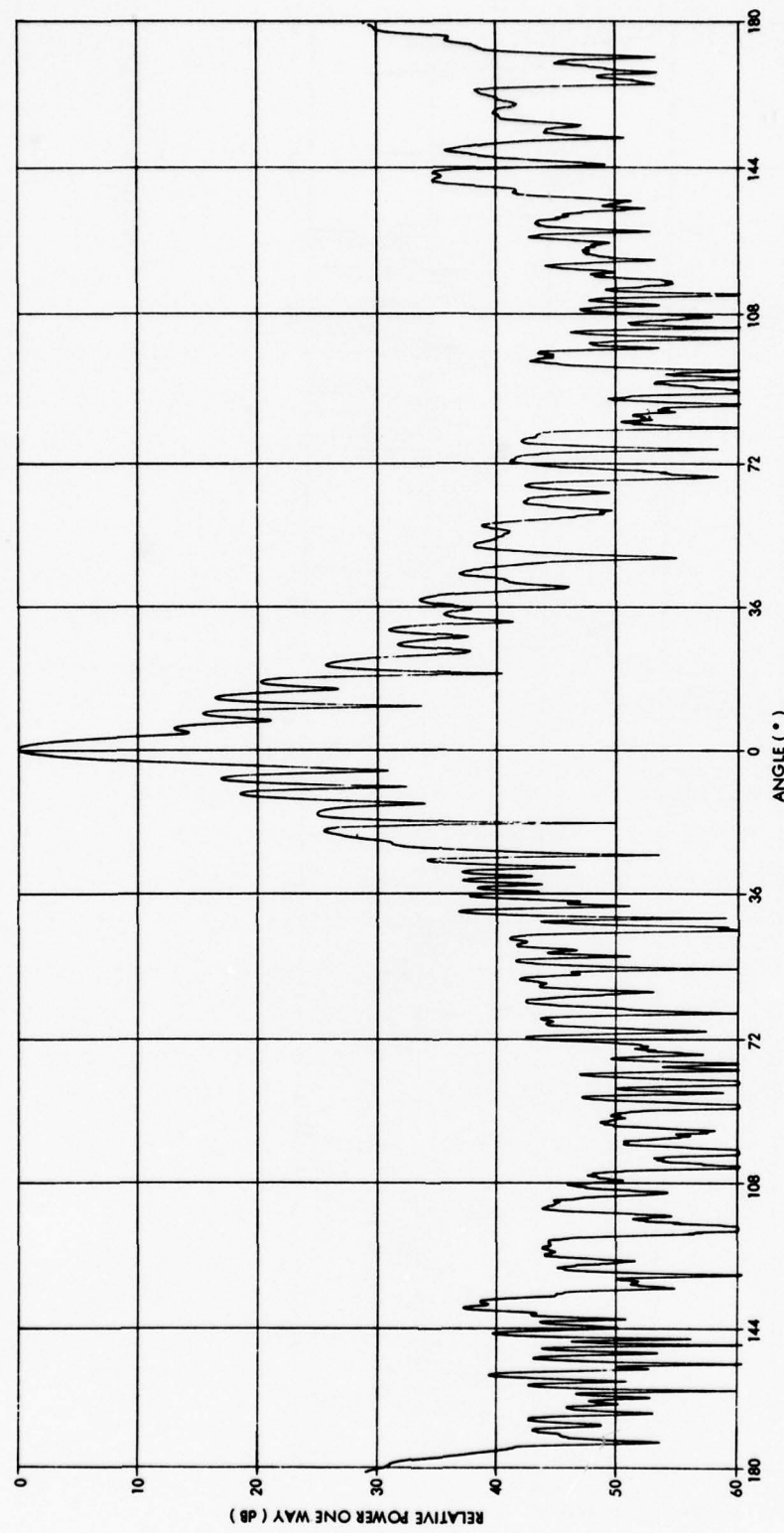


Figure 26 - H-Plane Modified Linear Array Pattern With Filter 1, 9.33 GHz

UNCLASSIFIED



39/4c
UNCLASSIFIED

Figure 27 - H-Plane Modified Linear Array Pattern with Filter 1, 9.5 GHz

Figure 28 - H-Plane Modified Linear Array Pattern With Filter 1, 9.69 GHz

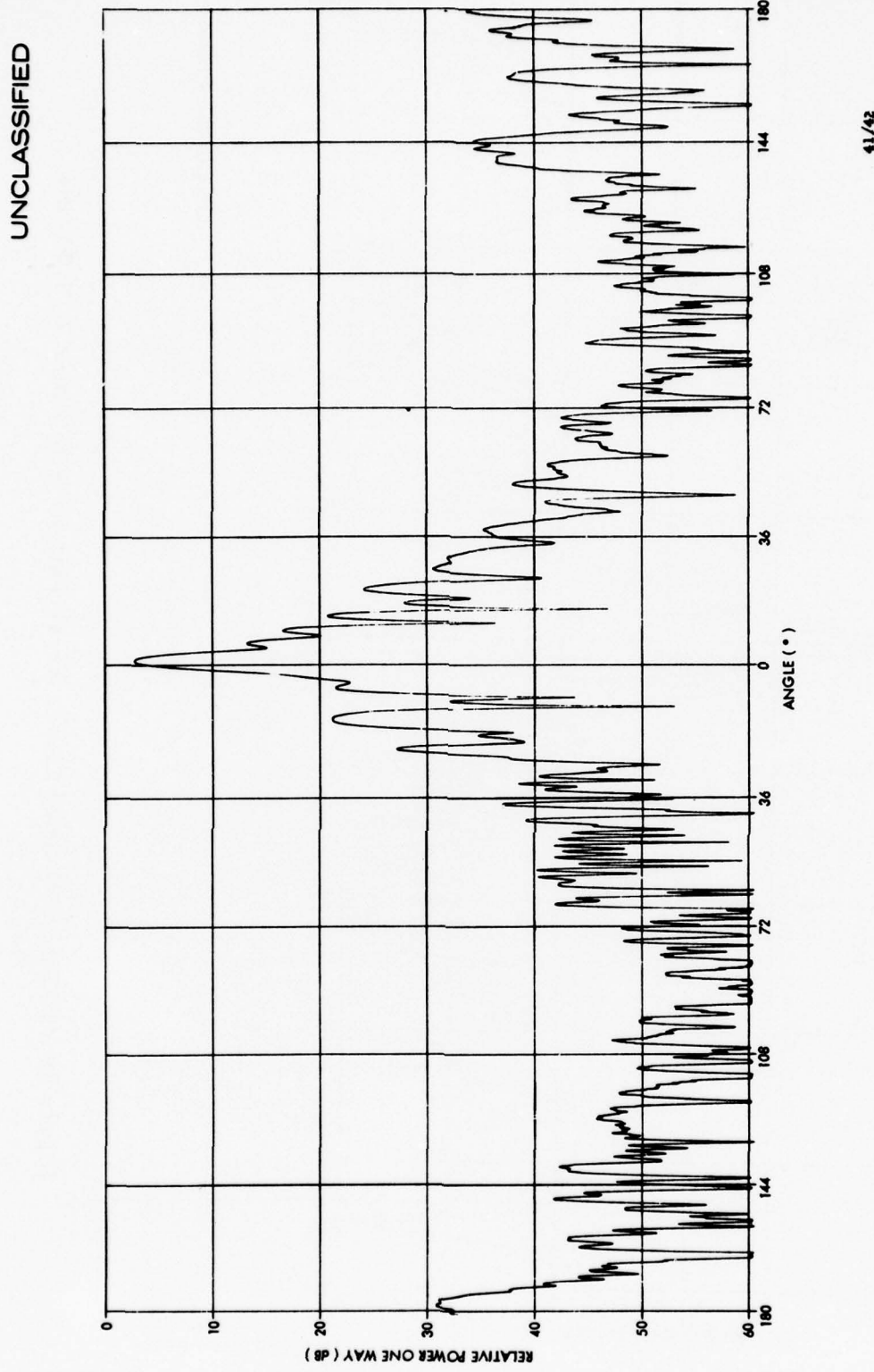


Figure 29 - H-Plane Modified Linear Array Pattern With Filter 2, 9.33 GHz

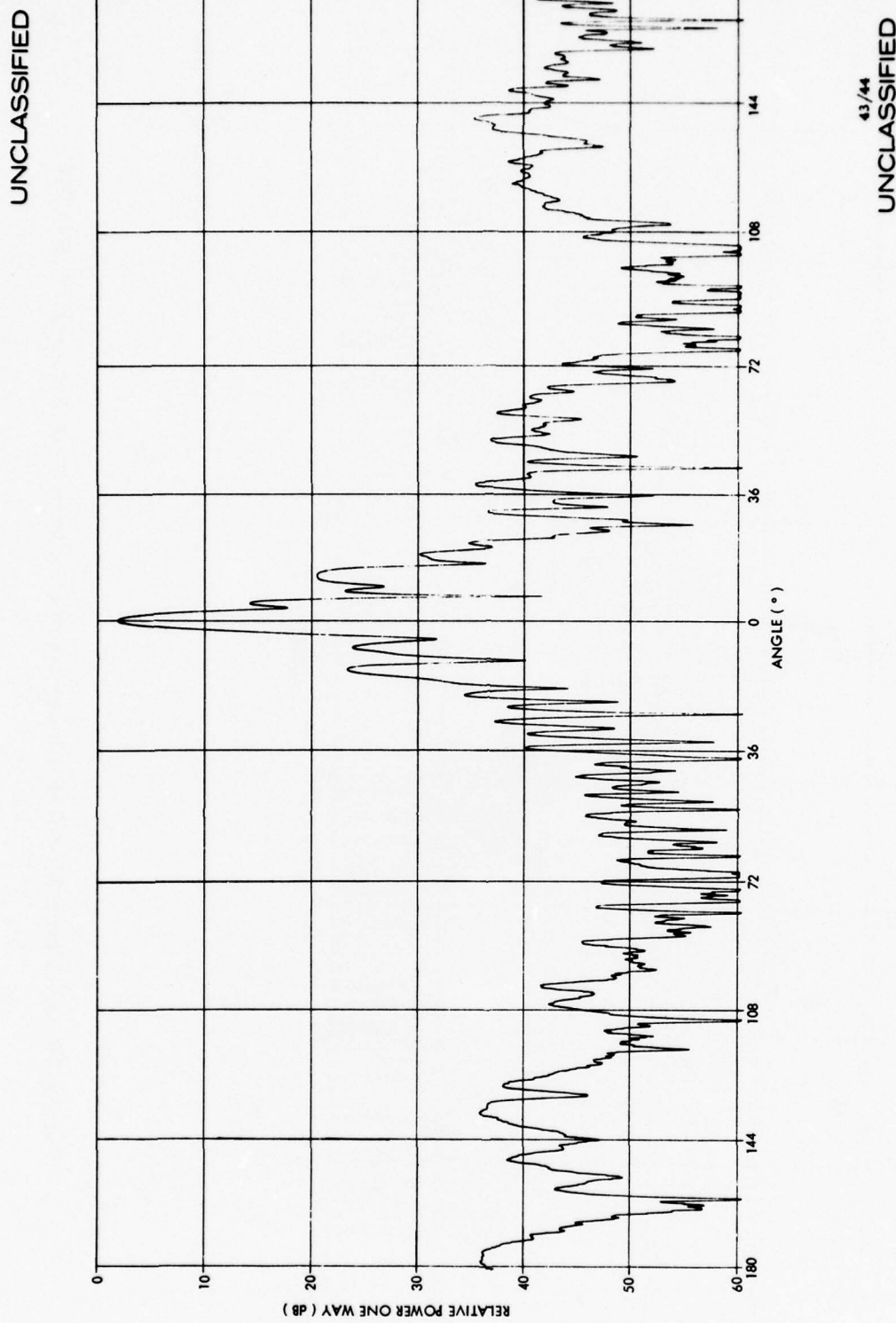
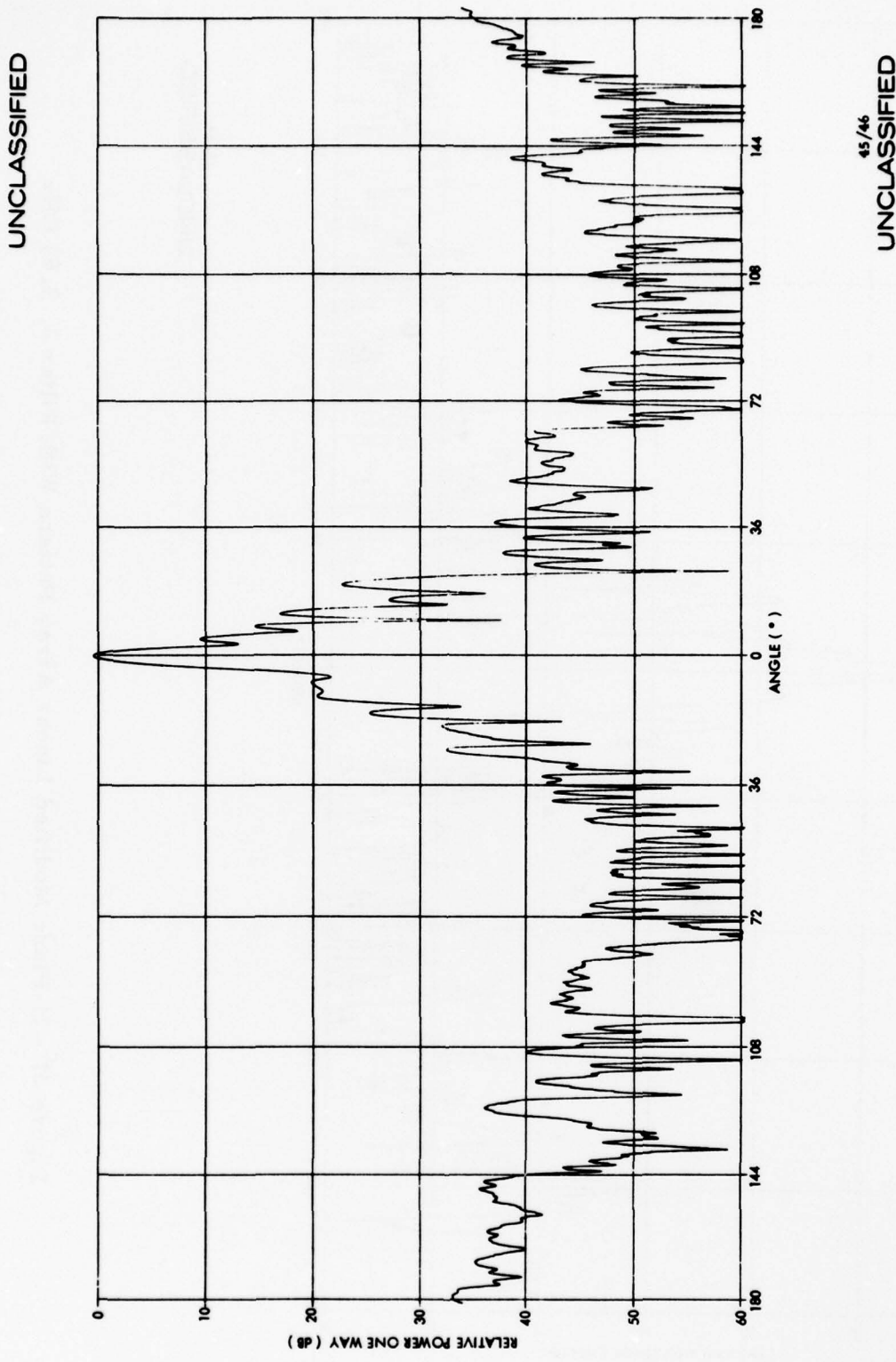


Figure 30 - H-Plane Modified Linear Array Pattern With Filter 2, 9.5 GHz



UNCLASSIFIED

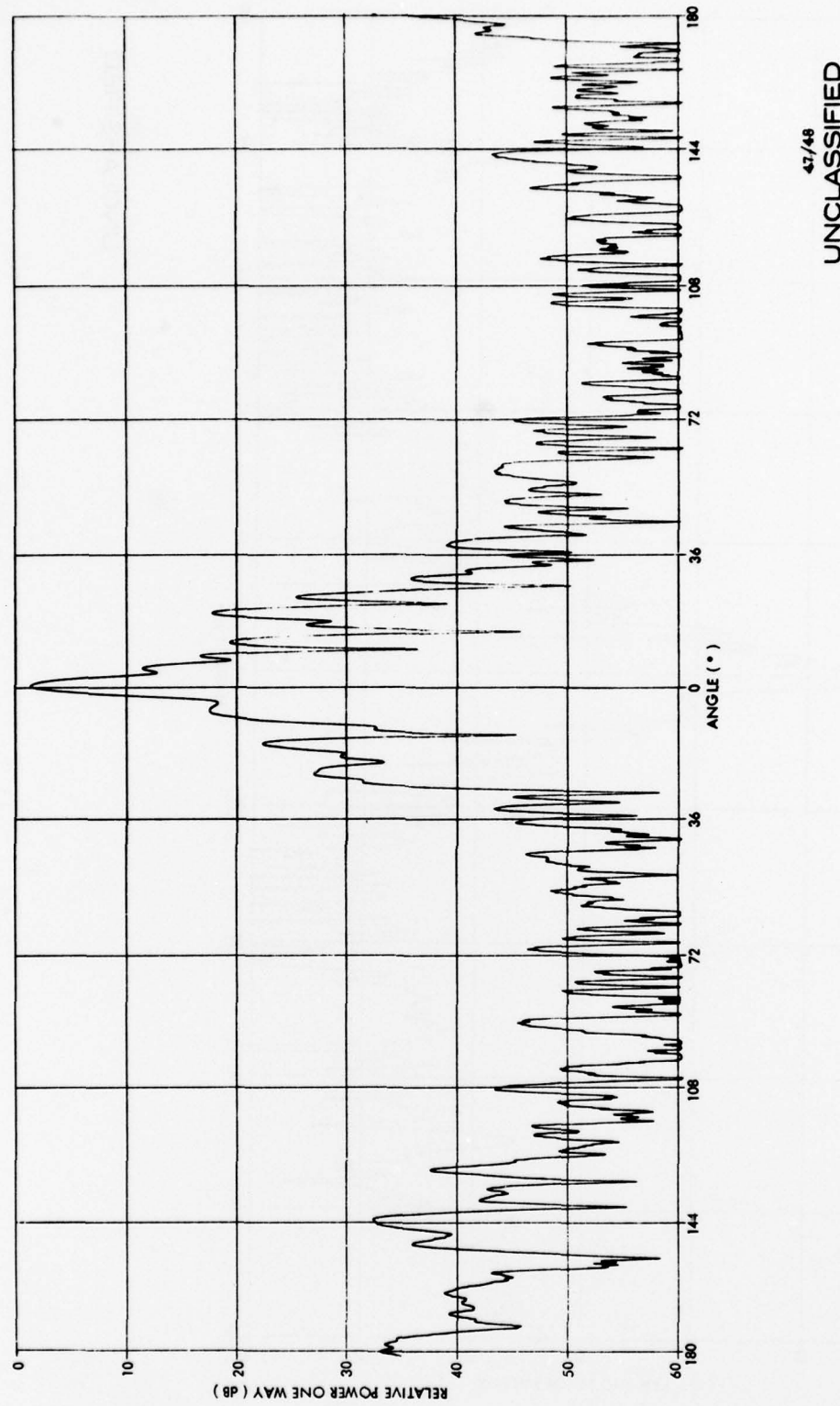
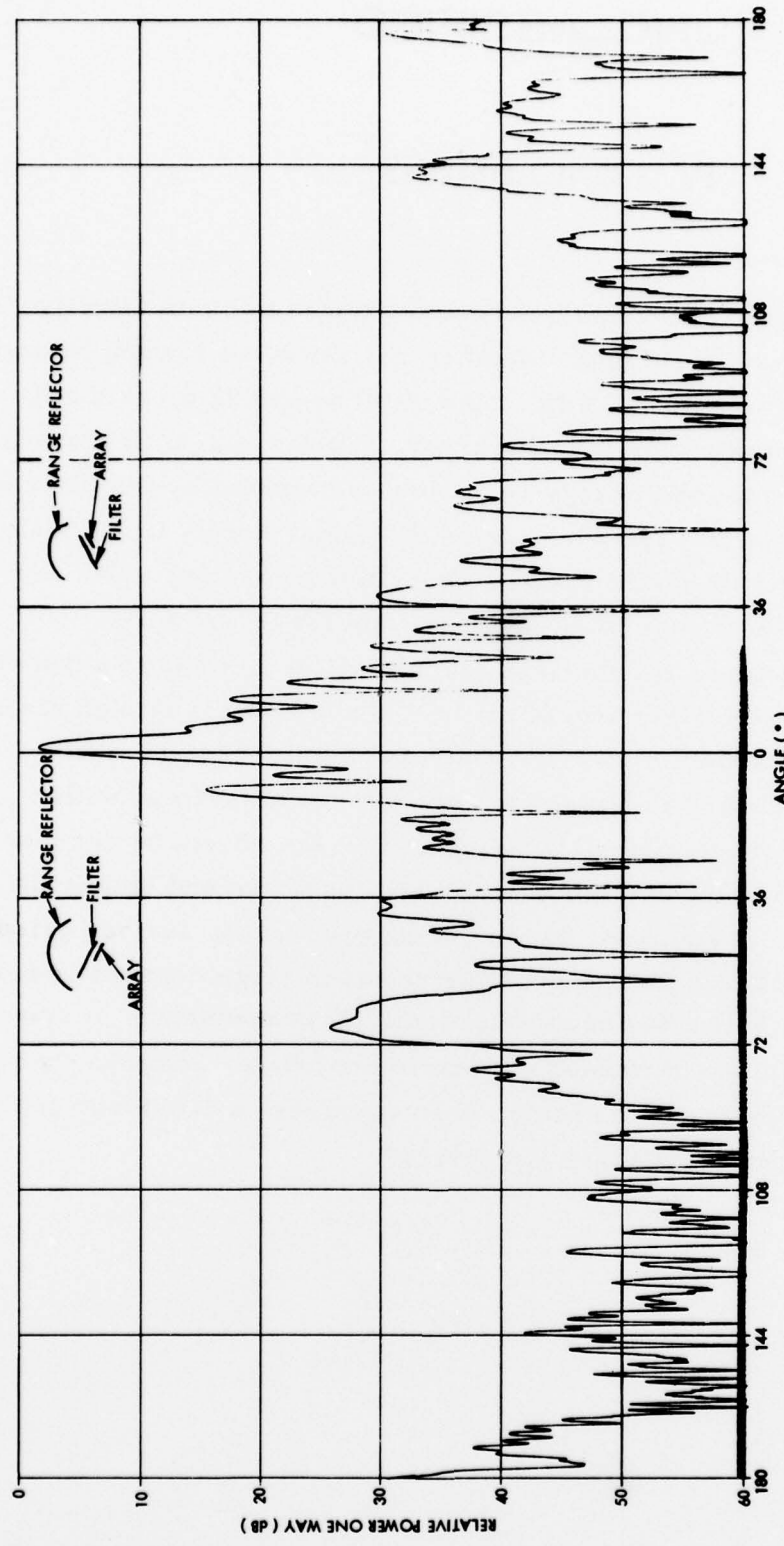


Figure 31 - H-Plane Modified Linear Array Pattern With Filter 2, 9.69 GHz

43/48
UNCLASSIFIED

UNCLASSIFIED



43
UNCLASSIFIED

Figure 32 - E-Plane Modified Linear Array Pattern With Filter 1, 9.5 GHz

UNCLASSIFIED

IV. CONCLUSIONS

The dielectric spatial filter has been demonstrated to be an effective means of controlling far out antenna sidelobes and unwanted grating lobes. Grating lobe rejection exceeding 32 dB in the H-plane and 22 dB in the E-plane has been demonstrated for a linear array. Furthermore, it has been demonstrated that grating lobe energy reactively terminated by the filter may appear either at the antenna feed port, or as additional energy in the main beam. A particular result has been cited wherein 6 dB grating lobes are rejected to the 29 dB level, and main beam gain increased by 3 dB.

The fabrication process for the experimental filter has shown several key areas which require further investigation. The synthesis of high dielectric constant multicomponent materials poses potential tolerance difficulties. Significant changes in dielectric constant and anisotropy within single large sheets of these materials requires that the sheets be cut into small tiles to randomize the buildup of transmission phase and amplitude error over the filter. In addition, due to curing processes, surface grinding of multicomponent synthetic dielectrics may result in large changes in permittivity (6.6 percent error has been observed). In consequence, it appears that the primary advantage of molded dielectric materials, namely, that they can be fabricated as large single sheets, is in actuality, a disadvantage if more than one sheet per filter layer is required.

UNCLASSIFIED

UNCLASSIFIED

APPENDIX A
EMERSON & CUMING, INC. TEST REPORT

This Appendix presents the Emerson & Cuming, Inc. final test report on the synthesized dielectric materials in its entirety, and, without comment.

UNCLASSIFIED

UNCLASSIFIED

November 12, 1977

RAYTHEON COMPANY
Hartwell Road
Bedford, MA. 01730

Attention: Mr. Jerome Posgay

Subject: Purchase Order No. 71-3407BB-92098, Dielectric Filter
Sandwich per Sketch No. RH-6677BB-100.

Gentlemen:

On November 7, 1977 the subject sandwich was shipped to you in accordance with subject purchase order. The order also requires a test report. This letter is the test report and completes our obligations under the purchase order.

The final dimensions of the sandwich are:

Length: 46.38"
Width: 5.65"
Height: 7.68"

The dielectric constant of the spacer foam varied over a range from 1.022 to 1.021. This was at a test frequency of 9.5 GHz, which was the test frequency for all of the dielectric measurements.

All of the dielectric measurements were made on a free space interferometer at 45° incidence, perpendicular polarization. Thus the electric field is in the plane of the sheets. Two measurements were made on each sheet, in one of which the electric field was along the length of the sheet, and in the other perpendicular to the length of the sheet. The 0° value is along the length of the sheet. The 90° value is perpendicular to the length.

In the thickness table which follows the sheets are numbered in order including the foam spacer layers. Each high dielectric layer is comprised of two dielectric sheets with the seam at the center. The foam

UNCLASSIFIED

UNCLASSIFIED

Raytheon Company Letter Test Report
Page 2

space layers have seams at locations other than the center. Two dielectric data tables are presented. The first gives dielectric values and thicknesses before machining to the final thicknesses which were optimized by Raytheon Company.

Final Sandwich Thickness Tabulation

<u>Layer</u>	<u>Design Thickness</u>	<u>Actual Thickness</u>
1 (K-5)	0.468"	0.466"
2 (Foam)	2.441"	2.438"
3 (K-9.7)	0.266"	0.268"
4 (Foam)	1.857"	1.874"
5 (K-23)	0.153"	0.154"
6 (Foam)	0.617"	0.612"
7 (K-23)	0.200"	0.200"
8 (Foam)	0.598"	0.603"
9 (K-9.7)	0.246"	0.247"
10 (Foam)	0.637"	0.630"
11 (K-5)	0.088"	0.088"

Preliminary Dielectric Data

<u>Sheet No.</u>	<u>Thickness</u> <u>Inches</u>	Relative Dielectric Constant	
		<u>0°</u>	<u>90°</u>
1	0.494	4.97	4.86
2	0.494	4.91	4.88
3	0.493	4.94	5.00
*4	0.345	4.97	4.95

*Note: Original Sheet lost during final surface grinding.

1	0.626	9.77	9.82
2	0.626	10.05	9.59
3	0.626	9.89	9.60
4	0.626	9.94	9.46
1	0.293	23.30	23.65
2	0.293	22.65	22.23
3	0.292	24.01	22.48
4	0.292	22.23	23.27

UNCLASSIFIED

UNCLASSIFIED

Raytheon Company Letter Test Report
Page 3

Final Dielectric Data

Sheet No.	Thickness Inches	Relative Dielectric Constant	
		0°	9.5 GHz
1	0.466	4.85	5.03
2	0.466	4.82	4.93
3	0.088	4.83	5.13
*4	0.088	5.10	4.95

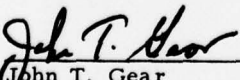
*Note: Original Sheet lost during final surface grinding.

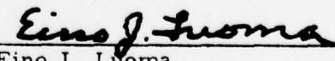
1	0.268	9.70	9.63
2	0.268	9.63	9.72
3	0.247	9.56	9.56
4	0.247	9.87	9.41
1	0.154	24.30	22.12
2	0.154	23.27	22.39
3	0.200	24.28	22.40
4	0.200	23.70	24.34

Comments and Recommendations

- 1) We recommend that the low dielectric constant spacer layer material have a somewhat higher density and dielectric constant than that chosen for this design. This would improve the structural performance of the sandwich without appreciably affecting the electrical performance. A foam with a dielectric constant of 1.06 and a density of 3.2 lbs/cu. ft. is recommended. The higher density would also improve the machinability of the spacer layers and the ability to maintain tight dimensional tolerances.
- 2) Since in these filter sandwich designs there is considerable flexibility available in the choices of the K's and thicknesses of the individual layers, it may be worthwhile to expend further effort on the theoretical side where emphasis is placed on considerations such as broad frequency range, minimum total thickness, minimum weight, optimum structural properties, and lowest incidence angle cut-off.

It has been a pleasure to participate with Raytheon Company in this sandwich program. We look forward to future programs such as this, and we believe that these sandwiches will become a useful accessory or addition to future antennas.


John T. Gear
Engineering Assistant


Eino J. Luoma
Chief Physicist

JTG/EJL:cw

cc: CLE, RAN, PEF, EJL, EFB

UNCLASSIFIED

APPENDIX B DIELECTRIC SPATIAL FILTER COUPLING TO PLANAR ARRAYS OF CIRCULAR ELEMENTS

It has been demonstrated by Fante⁽³⁾ that the filtering properties of infinite planar dielectric spatial filters are independent of source location provided the source is far from the filter: that is, sufficiently far such that the filter does not alter the current distribution at the source. Typically, this might be of the order of $\lambda/4$ separation. The remaining question, then, is what is the interaction between filter and source when the separation is less than, say, λ .

This question is quite broad, but may be succinctly treated when the source consists of an infinite planar array of identical apertures in a uniform grid. Borgiotti⁽⁶⁾ demonstrated for an infinite planar array of apertures, that the modal aperture admittance (looking out) has the general form

$$Y_i(\underline{u}_o) = \sum_{pq} Y^{TM}(\underline{u}_{pq}) |\&_{\rho i}(\underline{u}_{pq})|^2 + Y^{TE}(\underline{u}_{pq}) |\&_{\psi i}(\underline{u}_{pq})|^2 \quad (B-1)$$

where \underline{u}_o is the spectral component in the scan direction; \underline{u}_{pq} is the spectral component of the pqth Floquet harmonic; $\&_{\rho i}(\underline{u}_{pq})$ and $\&_{\psi i}(\underline{u}_{pq})$ are the TM and TE components, respectively, of the vector Fourier transform of the ith aperture mode; and $Y^{TM}(\underline{u}_{pq})$ and $Y^{TE}(\underline{u}_{pq})$ are the TM and TE Floquet modal admittances of the pqth spectral order looking outward from the aperture plane.

Borgiotti⁽⁴⁾ further demonstrated that for a single layer dielectric covering of thickness d and relative permittivity ϵ_r on the array, the aperture modal admittance is obtained by replacing $Y^{TM}(\underline{u}_{pq})$ and $Y^{TE}(\underline{u}_{pq})$ by the input admittance of the equivalent transmission line circuit in Figure B-1 for each spectral order. The extension to multiple layers is obvious. In a straight-forward manner it is then possible to solve for the reflection and transmission coefficients of an array/filter combination and to study the effects of proximity on performance.

UNCLASSIFIED

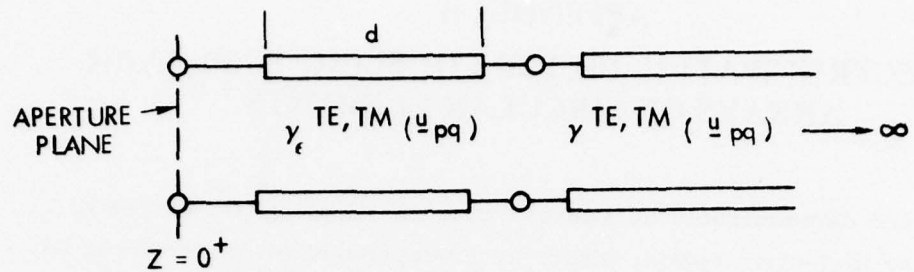


Figure B-1 - Equivalent Transmission Line Network for Spectral Orders of Unit Cell Waveguide

Figure B-2 shows the H-plane realized gain pattern of an array of loaded circular apertures with and without an eleven layer dielectric spatial filter at band center (the filter configuration is shown in Figure 1 of the text). The array is matched to broadside in the free space environment. With the filter butted directly to the aperture plane, the overall performance is

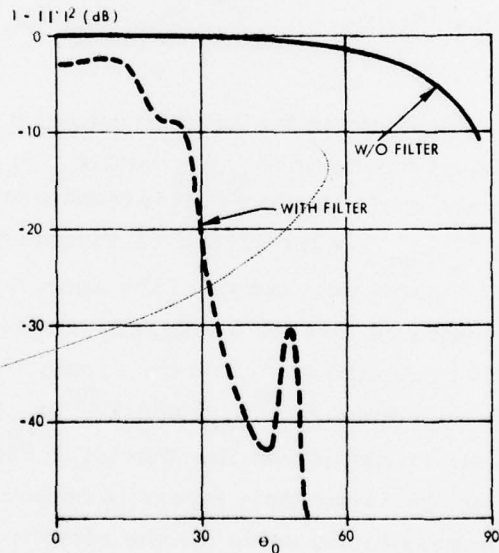


Figure B-2 - H-Plane Realized Gain Pattern With and Without Preliminary Design Eleven-Layer Filter - 9.5 GHz Array Matched to Free Space
50

UNCLASSIFIED

UNCLASSIFIED

severely degraded, although, by comparison with Figure 2 of the text, the basic filter spatial characteristic is maintained. By matching the array to broadside in the filter environment, the filter response is recovered, as shown in Figure B-3. Consequently one may conclude that for a given filter, and given grating lobe free array configuration, a matching structure can be determined (at least in principle) which will result in the desired filter response for any filter/array separation. It is equally clear that, again in the absence of grating lobes, a filter/array spacing can be determined for a free space matched array such that the filter does not interact (reactively) with the array. This last is, of course, exactly the conclusion reached by Fante⁽³⁾.

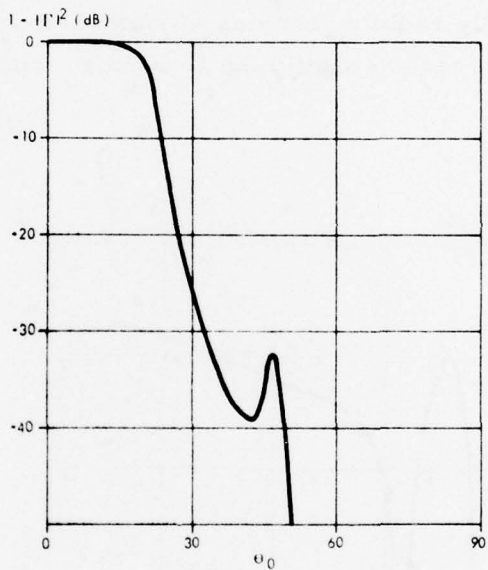


Figure B-3 - H-Plane Realized Gain Pattern with Preliminary Design
Eleven-Layer Filter - 9.5 GHz - Array Matched to Filter

In the instance that an array supporting grating lobes is used in conjunction with a dielectric spatial filter, the situation is somewhat more complex, since, in general, for the particular grid configuration the filter would be specifically designed to reject the unwanted beams. In this case the filter reactively terminates the grating lobes, and the array/filter spacing becomes

UNCLASSIFIED

UNCLASSIFIED

a significant variable. Since the spurious beams are propagating, the influence of array/filter spacing on aperture mismatch and main beam gain must fluctuate as the reflected beams phase in and out at the aperture plane. This is illustrated in Figure B-4 which shows $1 - |\Gamma|^2$ for broadside scan as a function of array/filter separation for an array supporting grating lobes. The filter is the eleven layer design shown in Figure 1 of the text. The array grid is rectangular with E-plane spacing of 0.75λ and H-plane spacing of 1.618λ , corresponding to H-plane grating lobes at $\pm 38.2^\circ$ in the broadside scan condition. The array is not matched. Without the filter, all beams are equally excited. With the filter present, $1 - |\Gamma|^2$ is approximately equal to the normalized power in the main beam.

With the array directly butted against the filter, the filter totally mismatches the array. As the separation increases, $1 - |\Gamma|^2$ rapidly increases out to 0.05λ , then equally rapidly becomes mismatched again. Beyond 0.1λ , the mismatch decreases steadily out to 0.35λ , where the calculations

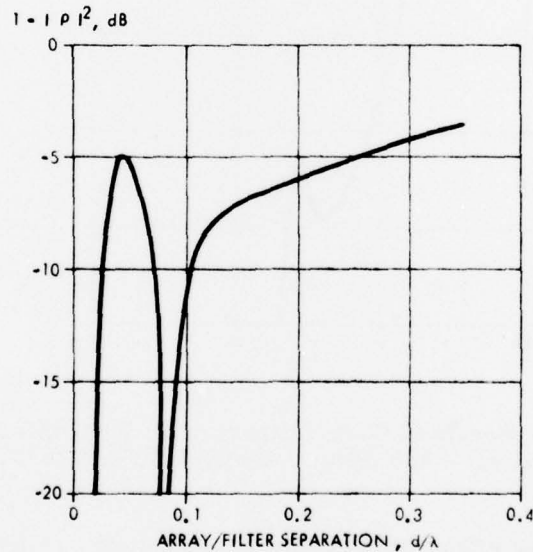


Figure B-4 - $1 - |\Gamma|^2$ Versus Array/Filter Separation
for an Array Supporting Grating Lobe -
Preliminary Design Eleven-Layer Filter - 9.5 GHz

UNCLASSIFIED

were terminated. It is interesting to note that for separations $0.17\lambda \leq d \leq 0.350$, the power in the main beam is greater with the filter present than without. This is not at all unreasonable when one considers that the power in the grating lobes can only appear at the feed port or in the main beam.

Although the calculations were not carried beyond 0.350λ separation, it is not unreasonable to assume that the array match is periodic with filter/array separation. The only mechanism by which the grating lobe energy can be transferred to the main beam is via reflection at the array face.

UNCLASSIFIED

UNCLASSIFIED

REFERENCES

- 1) Pozgay, J. H., Zamoscianyk, S., and Lewis, L. R., "Synthesis of Plane Stratified Dielectric Slab Spatial Filters Using Numerical Optimization Techniques", Final Report, Contract F19628-76-C-0189, December 1976.
- 2) Luoma, E. J., "Anisotropy in Dielectric Materials", Insulation/Circuits, 1971.
- 3) Fante, R. L., "Effects of Location on the Effectiveness of Spatial Filters", Report No. RADC-TR-76-296, September, 1976.
- 4) Borgiotti, G. V., "A Novel Expression for the Mutual Admittance of Planar Radiating Elements", IEEE Trans Antennas and Propagation, May, 1968.
- 5) Abramowitz, M., and Stegun, I. A., Handbook of Mathematical Functions, Dover, N. Y., pg. 231.
- 6) Borgiotti, G. V., "Modal Analysis of Periodic Planar Phased Arrays of Apertures", IEEE Proc., Vol. 56, No. 11, November, 1968, pp 1881-1892.

UNCLASSIFIED

***MISSION
of
Rome Air Development Center***

RADC plans and conducts research, exploratory and advanced development programs in command, control, and communications (C³) activities, and in the C³ areas of information sciences and intelligence. The principal technical mission areas are communications, electromagnetic guidance and control, surveillance of ground and aerospace objects, intelligence data collection and handling, information system technology, ionospheric propagation, solid state sciences, microwave physics and electronic reliability, maintainability and compatibility.